Journal of Neuroinflammation

RESEARCH

Open Access

Fucoidan reduces NET accumulation and alleviates chemotherapy-induced peripheral neuropathy via the gut–blood–DRG axis

Rumeng Jia[1†], Li Wan[2†], Lai Jin[1†], Qingyan Tian[1], Yongyi Chen[5], Xia Zhu[4], Mengyao Zhang[1], Yajie Zhang[3], Lijuan Zong[1], Xuefeng Wu[2], Chen Miao[6], Yihang Cai[1], Jianxin Ma[4*], Liang Hu[1*] and Wen-Tao Liu[1*]

Abstract

Background Chemotherapy-induced peripheral neuropathy (CIPN) is a serious adverse reaction to chemotherapy with limited treatment options. Research has indicated that neutrophil extracellular traps (NETs) are critical for the pathogenesis of CIPN. LPS/HMGB1 serve as important inducers of NETs. Here, we aimed to target the inhibition of NET formation (NETosis) to alleviate CIPN.

Methods Oxaliplatin (L-OHP) was used to establish a CIPN model. The mice were pretreated with fucoidan to investigate the therapeutic effect. SR-A1$^{-/-}$ mice were used to examine the role of scavenger receptor A1 (SR-A1) in CIPN. Bone marrow-derived macrophages (BMDMs) isolated from SR-A1$^{-/-}$ mice and WT mice were used to investigate the mechanism by which macrophage phagocytosis of NETs alleviates CIPN.

Results Clinically, we found that the contents of LPS, HMGB1 and NETs in the plasma of CIPN patients were significantly increased and positively correlated with the VAS score. Fucoidan decreased the LPS/HMGB1/NET contents and relieved CIPN in mice. Mechanistically, fucoidan upregulated SR-A1 expression and promoted the phagocytosis of LPS/HMGB1 by BMDMs. Fucoidan also facilitated the engulfment of NETs by BMDMs via the recognition and localization of SR-A1 and HMGB1. The therapeutic effects of fucoidan were abolished by SR-A1 knockout. RNA-seq analysis revealed that fucoidan increased sqstm1 (p62) gene expression. Fucoidan promoted the competitive binding of sqstm1 and Nrf2 to Keap1, increasing Nrf2 nuclear translocation and SR-A1 transcription. Additionally, the sequencing analysis (16 S) of microbial diversity revealed that fucoidan increased the gut microbiota diversity and abundance and increased the Bacteroides/Firmicutes ratio.

†Rumeng Jia, Li Wan and Lai Jin contributed equally to this work.

*Correspondence:
Jianxin Ma
mjx3416@163.com
Liang Hu
lianghu@njmu.edu.cn
Wen-Tao Liu
painresearch@njmu.edu.cn

Full list of author information is available at the end of the article

Conclusions Altogether, fucoidan promotes the SR-A1-mediated phagocytosis of LPS/HMGB1/NETs and maintains gut microbial homeostasis, which may provide a potential therapeutic strategy for CIPN.

Graphical Abstract

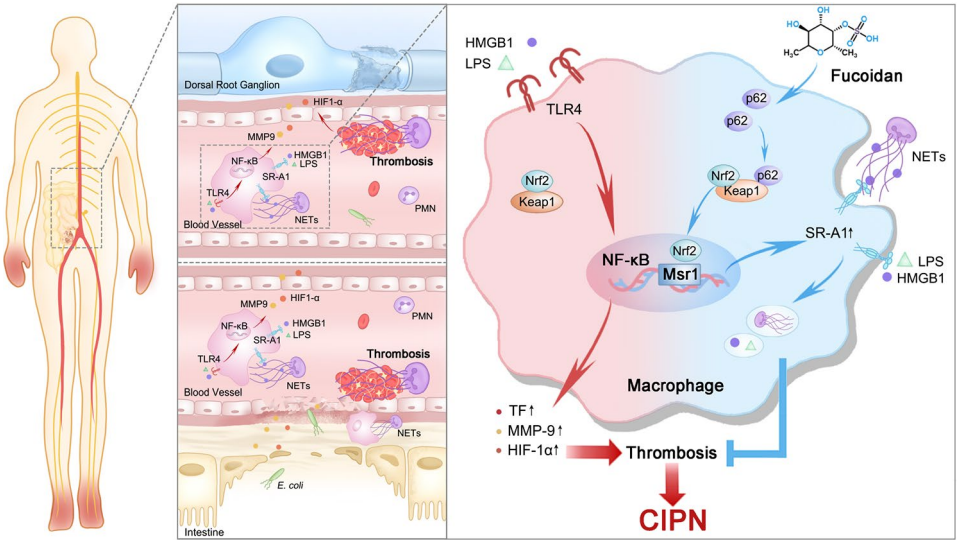

Keywords NETs, CIPN, Fucoidan, SR-A1, Macrophage, Gut

Introduction

Current treatment modalities for cancer include surgical interventions, radiotherapy, and chemotherapy drug regimens, although they are often accompanied by severe adverse effects. These drugs frequently elicit sensory receptor stimulation and damage, precipitating CIPN and profoundly impacting treatment efficacy and patients' quality of life. The clinical symptoms of CIPN include limb numbness, hyposensitivity, abnormal feelings, and pain, with an incidence rate of over 70% [1–3]. According to a survey by the American Association of Clinical Oncology, the only recommendation for CIPN is to suspend or delay chemotherapy [3, 4]. Therefore, an exploration of the pathological mechanism of CIPN and the development of new treatments are urgently needed.

Neutrophil extracellular traps (NETs) are fibrous networks that protrude from the membranes of activated neutrophils. NETs are found in a variety of conditions, such as infection, malignancy, atherosclerosis, and autoimmune diseases [5]. Research has revealed that in patients with COVID-19 [6], NETs have the potential to trigger immune thrombosis, which is a critical pathological mechanism of ARDS and can lead to pulmonary circulation disorders [7]. A previous study revealed that neutrophils invade sensory ganglia and confer mechanical hypersensitivity in fibromyalgia mice [8]. Additionally, our previous research indicated that NETs play an important role in the development of CIPN. They mediate neuroinflammatory responses and cause microcirculation disorders at nerve endings, leading to pain hypersensitivity. Reducing NET-mediated inflammation could be an effective strategy for mitigating CIPN [9]. Promising therapeutic effects have also been observed with the use of DNase 1 to degrade NETs [10]. However, considering that the application of DNase in clinical settings may produce immunogenic reactions and pose challenges for clinical translation, we are exploring other treatment strategies. Here, we aimed to investigate whether targeting the source of NET production can effectively treat CIPN.

Research has shown that the factors that induce NET formation include p-selectin, HMGB1, fungi, bacteria, and immune complexes [11]. Among them, HMGB1 and bacterial LPS have attracted our attention. Previous reports have indicated that NET formation (NETosis) depends on PAMPs (lipopolysaccharide, LPS) and DAMPs (HMGB1), which can stimulate neutrophils, leading to the release of NETs [12–14]. Studies have shown that intestinal flora disorders are closely related to neuropathic pain [15]. Jianren Mao et al. confirmed LPS release induced by a disordered intestinal microbiota could promote mechanical hyperalgesia caused by chemotherapy [16]. Additionally, intrathecal treatment with the TLR4 antagonist lipopolysaccharide-RS (LPS-RS) blocked mechanical hypersensitivity in paclitaxel-treated rats [17]. Previous reports have shown that the excessive accumulation of HMGB1 is a crucial cause of neuropathic pain [18–21]. Recently, Jon D. Levine et al.

reported that DAMPs are ligands for pattern recognition receptors (PRRs) and that PRRs in DRG cells play important roles in CIPN [22]. These findings suggest that LPS/HMGB1, as important factors for triggering NET formation, may be involved in the process of CIPN.

Therefore, we aimed to reduce the accumulation of LPS/HMGB1 and decrease their stimulation of neutrophils to inhibit NET production. A decrease in the LPS/HMGB1 levels in the body is due to the inflammatory response caused by binding to corresponding endogenous ligands, such as TLR/RAGE, while LPS/HMGB1 is also taken up and eliminated by phagocytic cells [19, 23, 24]. We hypothesized that phagocytic receptors can be regulated to promote the clearance of LPS/HMGB1 to alleviate CIPN. Here, we detected several LPS/HMGB1-related recognition receptors on macrophage surfaces after L-OHP stimulation. The screening results revealed that the SR-A1 receptor was significantly downregulated in the L-OHP group. SR-A1 is an important pattern recognition receptor in innate immunity that can recognize LPS/HMGB1 [19, 25]. However, whether SR-A1 is related to the phagocytosis of LPS/HMGB1 to inhibit NET formation in CIPN is unclear.

In the process of exploring the involvement of SR-A1 in the pathogenesis of CIPN, we also sought to develop an effective method for regulating SR-A1 to alleviate CIPN. Fucoidan is the main component of the clinical drug Haikunshenxi, which is used to treat chronic renal failure and has good anti-inflammatory effects. It is a unique water-soluble polysaccharide with a sulfuric acid group that has been shown to treat hypertension in obese subjects by upregulating SR-A1 [26]. However, its role in CIPN has not yet been reported. Studies have shown that fucoidan has anticoagulant and antithrombotic effects [27, 28] and is protective for the intestine [29]. Therefore, we speculate that fucoidan may alleviate CIPN.

Materials and methods

The study was reviewed and approved by the Nanjing First Hospital Institutional Review Committee with ethics number KY20171228-KS-01. All the experimental methods were conducted in accordance with the relevant guidelines and regulations. The experimental plan involving animals was approved by the Committee of Experimental Animal Ethics of Nanjing Medical University through the "Examination of Ethical Welfare of Experimental Animals" and complied with relevant national welfare ethics provisions for experimental animals. The approval number is IACUC-2,011,040. For each experiment, the number of mice, statistical analyses, and numbers of experimental replicates are described in the figure legends. All the cells used were cultured and handled according to the required protocols. Data processing and analysis involve statistical analyses of the results obtained from various experiments. The results are presented as the means ± SEMs, and p values < 0.05 were considered significant. A detailed description of the materials and methods is provided in the Supplemental Methods.

The RNA sequencing datasets presented in this study have been deposited in the NCBI Gene Expression Omnibus database at https://www.ncbi.nlm.nih.gov/, reference number GEO GSE249275.

Results

CIPN is accompanied by the excessive accumulation of LPS/HMGB1/NETs in the blood and microcirculation disorders

The content of histone H3 (H3Cit, a marker for NET formation) in the plasma of cancer patients before and after chemotherapy was measured to validate the critical role of NETs in CIPN. As shown in Fig. 1A, the accumulation of H3Cit in the blood increased after chemotherapy. Further analysis revealed a positive correlation between the H3Cit contents and VAS scores of CIPN patients (Fig. 1B). Studies have established a role for NET formation in promoting coagulation, vascular occlusion, and thrombosis [30, 31]. We previously reported a significant increase in TF expression in CIPN mice, resulting in microcirculatory disorders [10]. Here, we further confirmed that chemotherapy led to the accumulation of TF in the blood of CIPN patients (Fig. 1C), accompanied by a decrease in hand blood circulation. As the number of chemotherapy cycles increased, ischaemia in the limbs intensified (Fig. 1D and E). As is well known, "no obstruction, no pain." The evidence suggests that NETs serve as scaffolds for DNA with associated cytotoxic proteins and proteases, such as matrix metalloproteinase 9 (MMP9) [32]. Previous studies revealed that MMP9, an indicator of pain occurring downstream of TF, is involved in CIPN development [33]. We detected obvious increase in MMP9 activity in the plasma of CIPN patients (Fig. 1F). The formation of NETs is an important pathological mechanism underlying CIPN. Thus, restraining NET formation at the source is highly important. Research has shown that HMGB1 and LPS act on Toll-like receptor 4 (TLR4), promoting the formation of NETs [9, 13, 14]. Previous experimental results indicated that LPS derived from the intestine plays a crucial role in triggering NET formation [10], while HMGB1 accumulates significantly during the process of tumour dissolution during chemotherapy [19]. We believe that LPS/HMGB1, critical inducers of NET formation, actively promote the progression of CIPN. As depicted in Fig. 1G and H, LPS levels in the plasma of cancer patients increased significantly after chemotherapy and were positively correlated with VAS scores. Furthermore, we verified that chemotherapy led to the substantial accumulation of HMGB1 (Fig. 1I), which was positively correlated with patients'

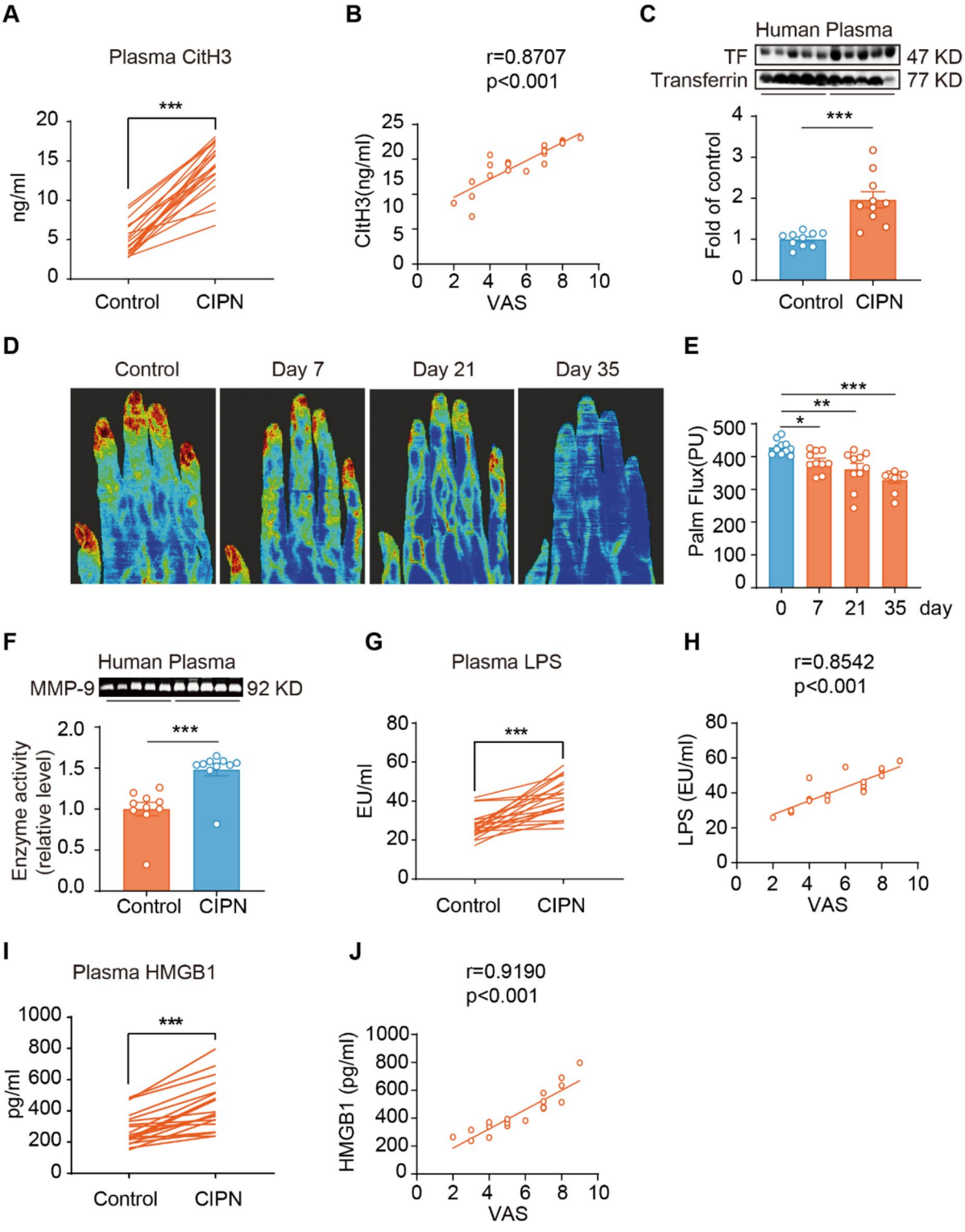

Fig. 1 (See legend on next page.)

(See figure on previous page.)

Fig. 1 CIPN is accompanied by the excessive accumulation of LPS/HMGB1/NETs in the blood and microcirculation disorders. (**A**) ELISA was used to detect the content of H3Cit in the plasma of patients with tumours before chemotherapy (control) and after chemotherapy (CIPN) ($n=20$). (**B**) After the last chemotherapy session, the correlation between the plasma H3Cit concentration and VAS score of CIPN patients was investigated ($n=20$). (**C**) western blotting was performed to detect the content of TF in the plasma of patients with tumours before and after chemotherapy ($n=10$). (**D**) (**E**) Investigation of hand blood flow in patients with tumours before chemotherapy and at 7, 21 and 35 days after chemotherapy by laser Doppler imaging ($n=10$). (**F**) A gelatine zymogram was used to investigate the activity of MMP9 in the plasma of patients with tumours before and after chemotherapy ($n=10$). (**G**) (**I**) ELISAs were used to detect the contents of LPS and HMGB1 in the plasma of patients with tumours before chemotherapy (control) and after chemotherapy (CIPN) ($n=20$). (**H**) (**J**) After the last chemotherapy session, the correlations between the plasma LPS/HMGB1 concentrations and the VAS scores of CIPN patients were investigated ($n=20$). Significant differences were determined using unpaired Student's t tests (**A**, **B**, **C**, **F**, **G** and **I**), one-way ANOVA (**E**) or linear regression analysis (**B**, **H** and **J**) (*$p<0.05$, **$p<0.01$ and ***$p<0.001$ compared with the control group)

pain ratings (Fig. 1J). These findings suggest that L-OHP causes the accumulation of NETs and microcirculatory disorders in CIPN patients, aggravates MMP9 activity, and that LPS/HMGB1 serve as essential upstream inducers of NET formation, contributing to the onset of CIPN.

L-OHP causes LPS/HMGB1/NET accumulation and microcirculatory disturbances in CIPN mice

A CIPN mouse model was established in B6/C57 mice via a continuous injection of the drug L-OHP (3 mg/kg, i.p.) for five days to further validate the pathological mechanisms of LPS/HMGB1/NET involvement in CIPN. L-OHP significantly induced mechanical hypersensitivity in mice (Fig. 2A) and increased the levels of H3Cit in the blood (Fig. 2B) and dorsal root ganglia (DRGs) (Fig. 2C and D). The formation of NETs caused hypercoagulability, the upregulation of tissue factor (Fig. 2E), disseminated intravascular coagulation in the body, and severe microcirculatory disturbances in the nerve endings and intestines (Fig. 2F-H), ultimately activating MMP9 (Fig. 2I) and promoting the development of CIPN. As previously reported, LPS is a critical inducer of NET formation. The content of LPS in mouse plasma and DRGs was measured. As shown in Fig. 2J, K and L-OHP increased the level of LPS accumulation in the plasma and DRGs. LPS, a gram-negative endotoxin and PAMP, primarily originates from the intestines [34, 35]. After chemotherapy, LPS in the blood may arise from damaged intestines. Haematoxylin–eosin staining revealed that L-OHP caused thinning of the intestinal wall and glandular atrophy in mice (Fig. 2L) and increased intestinal permeability (Fig. 2M). In addition to LPS, HMGB1 is also produced in large amounts during chemotherapy, and it participates in NET formation. We measured the levels of HMGB1 in mouse plasma and confirmed that L-OHP caused a significant increase in HMGB1 release (Fig. 2N). Consequently, the combined effects of LPS/HMGB1/NETs generated after chemotherapy lead to MMP-9 activation and microcirculatory disturbances, which are important pathological mechanisms of CIPN.

Dysfunction of SR-A1-mediated LPS/HMGB1 scavenging by macrophages induces CIPN

The decreases in LPS/HMGB1 levels result from an inflammatory response caused by their binding to corresponding endogenous ligands such as TLR/RAGE receptors; on the other hand, LPS is taken up and eliminated by phagocytic cells [19, 23, 24]. We extracted BMDMs from WT mice and stimulated them with L-OHP to further explore the mechanisms underlying the excessive accumulation of LPS/HMGB1. Recombinant FITC-LPS was added to the culture medium to investigate the phagocytosis of LPS by macrophages. The results shown in Fig. 3A indicate that the uptake of FITC-LPS by BMDMs decreased after L-OHP treatment. We also found that L-OHP inhibited the phagocytosis of FITC-HMGB1 (Fig. 3B). The mRNA levels of receptors on the macrophage membrane that can bind to LPS/HMGB1 were measured to investigate the reasons for the reduced ability of macrophages to phagocytose LPS/HMGB1. As shown in Fig. 3C, the mRNA levels of TLR4/TLR2 and other receptors related to the inflammatory signalling pathway were increased, whereas the expression of the scavenging receptor SR-A1 was decreased. We subsequently detected the level of the SR-A1 protein, as shown in Fig. 3D, and the expression of SR-A1 in BMDMs decreased significantly following L-OHP treatment. These results suggested that L-OHP could decrease SR-A1 expression and inhibit LPS/HMGB1 clearance by macrophages. In vivo, L-OHP also inhibited SR-A1 receptor expression in the intestinal tract and DRGs of the mice (Fig. 3E and F). SR-A1$^{-/-}$ mice were injected with a low concentration of L-OHP (1.5 mg kg, i.p.) for 5 days to establish the CIPN model to further investigate the importance of the SR-A1 receptor in CIPN. The results revealed that CIPN occurred more quickly and that mechanical pain was more severe in the SR-A1$^{-/-}$ mice than in the control mice (Fig. 3G). Furthermore, the shortening of the colon in the SR-A1$^{-/-}$ mice was more pronounced (Fig. 3H), suggesting that the intestine–nerve axis was involved in CIPN.

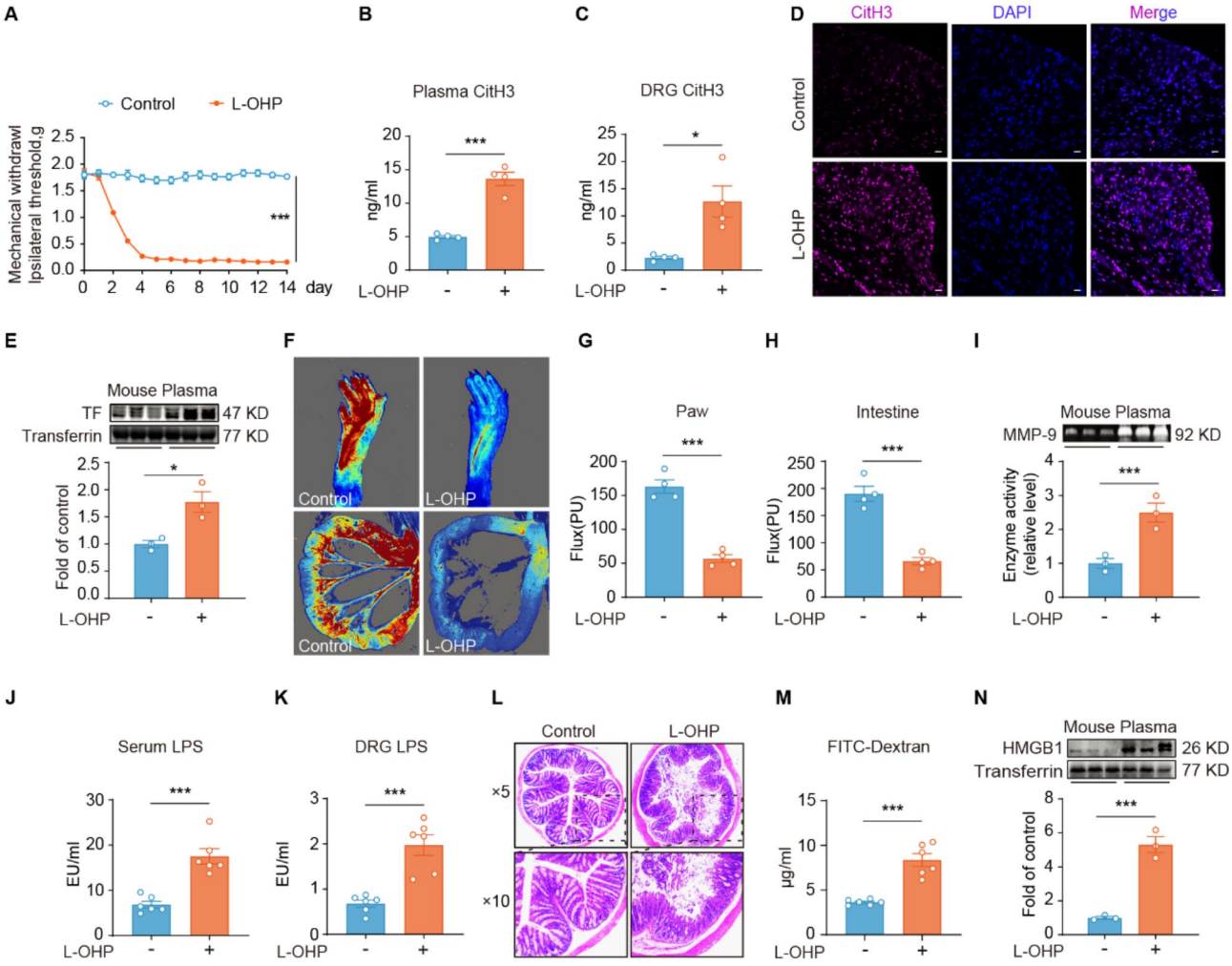

Fig. 2 L-OHP caused LPS/HMGB1/NET accumulation and microcirculatory disturbances in CIPN mice. (**A**) A CIPN model was established via the administration of L-OHP (3 mg/kg, i.p.) for 5 days. The mechanical pain threshold was detected in mice using the Von Frey test ($n=6$). (**B**) (**C**) The plasma and DRGs of the mice were collected on the 10th day after the first injection of L-OHP. The H3Cit content was detected by ELISA ($n=4$). (**D**) Immunofluorescence staining was performed to evaluate the expression of H3Cit in DRGs ($n=3$). Scale bar: 20 μm. (**E**) The TF levels in plasma were detected by western blotting ($n=3$). (**F**) (**G**) (**H**) The plantar microcirculatory condition and intestinal microcirculatory condition of the mice were investigated by laser Doppler imaging ($n=4$). (**I**) The activity of MMP9 in mouse plasma was detected by gelatine zymography ($n=3$). (**J**) (**K**) The content of LPS in the plasma and DRGs was detected via ELISA ($n=6$). (**L**) The intestinal tracts of the mice were fixed with 4% paraformaldehyde and subjected to HE staining ($n=3$). (**M**) On the 10th day after the first injection of L-OHP, FITC-dextran (600 mg/kg, i.g.) was administered to the mice. Four hours later, the serum of the mice was collected, and the concentration of FITC-dextran in the serum was detected using an enzyme labelling instrument ($n=6$). (**N**) HMGB1 expression in the plasma of the mice was detected by western blotting ($n=3$). Significant differences were determined using unpaired Student's t tests (**B**, **C**, **E**, **G**, **H**-**K**, **M** and **N**) or two-way ANOVA (**A**). (*$p<0.05$, **$p<0.01$ and ***$p<0.001$ compared with the control group)

Fucoidan upregulates SR-A1 expression in macrophages to clear LPS/HMGB1 and inhibits NET formation to alleviate CIPN

The deletion of the SR-A1 receptor accelerated CIPN after chemotherapy, and upregulating the expression of SR-A1 has become a key problem. Previous studies have shown that fucoidan can upregulate the expression of SR-A1 to alleviate the increase in obesity-related blood pressure [26]. However, the role of fucoidan in CIPN remains unexplored. The experimental procedure is shown in Fig. 4A. We found that fucoidan upregulated the expression of the SR-A1 receptor (Fig. 4B) and promoted the phagocytosis of FITC-LPS and FITC-HMGB1 by BMDMs (Fig. 4C and D). Furthermore, the phagocytic activity of BMDMs was assessed using fluorescent latex beads. As shown in Figure S2, L-OHP treatment impaired the phagocytic function of BMDMs, as evidenced by a marked reduction in the uptake of fluorescent latex beads compared with that in the control group. In contrast, fucoidan treatment effectively improved the phagocytic capacity of BMDMs. We performed an experiment in which LPS was used as a stimulus, either alone or in combination with fucoidan, to validate whether fucoidan affected phagocytosis in the context of LPS

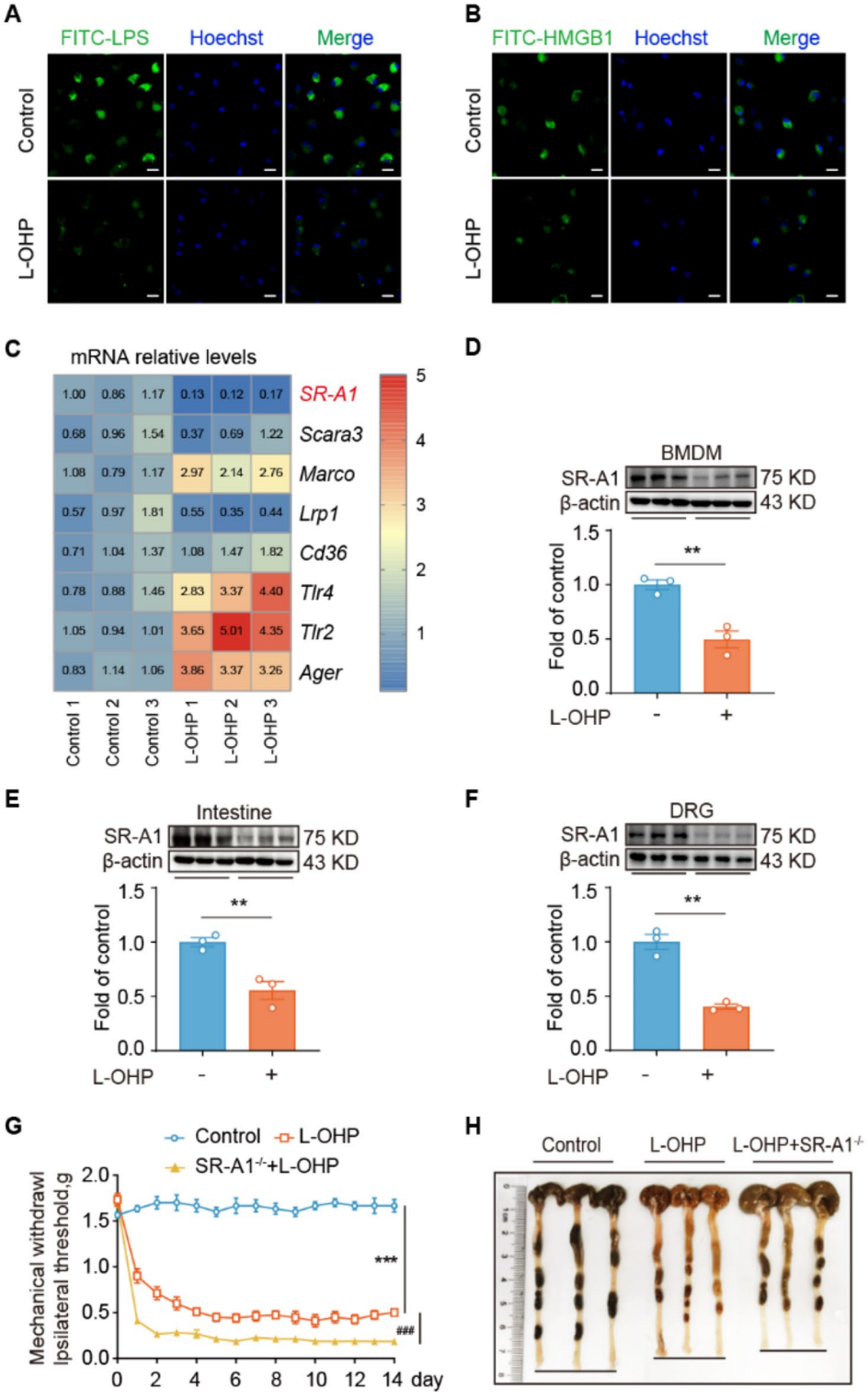

Fig. 3 (See legend on next page.)

(See figure on previous page.)

Fig. 3 Dysfunction of SR-A1-mediated LPS/HMGB1 scavenging by macrophages induced CIPN. (**A**) BMDMs were collected from WT mice and stimulated with L-OHP (5 μM) for 12 h. FITC-LPS (100 μg/ml) was added. The phagocytosis of FITC-LPS by BMDMs was observed under a confocal microscope ($n = 3$). Scale bar = 20 μm. The above conditions were repeated, and FITC-HMGB1 (10 nM) was added to observe its phagocytosis by BMDMs (**B**) ($n = 3$). Scale bar: 20 μm. (**C**) After BMDMs were obtained from WT mice and stimulated with L-OHP (5 μM) for 18 h, total RNA was extracted, and the mRNA levels of SR-A1, Scara3, Marco, LRP1, CD36, TLR4, TLR2, and RAGE were detected by qPCR ($n = 3$). (**D**) BMDMs were obtained from WT mice and stimulated with L-OHP (5 μM) for 18 h. The cells were collected, and the expression of SR-A1 was detected by western blotting ($n = 3$). The intestinal tract (**E**) and DRGs (**F**) of the mice were collected to investigate the expression level of SR-A1 ($n = 3$). (**G**) WT mice and SR-A1$^{-/-}$ mice were administered L-OHP (1.5 mg/kg, i.p.) for 5 days to establish a CIPN model. The Von Frey test was performed to detect the mechanical pain threshold of the mice ($n = 6$). (**H**) The intact colons of the mice were collected, and the colon lengths of the different treatment groups were compared ($n = 6$). Significant differences were determined using unpaired Student's t test (**C**-**F**) or two-way ANOVA (**G**). (*$p < 0.05$, **$p < 0.01$ and ***$p < 0.001$ compared with the control group)

exposure and to further investigate the impacts of LPS accumulation on macrophage phagocytic function and the potential ameliorative effects of fucoidan. As shown in Figure S3, LPS stimulation impaired BMDM phagocytosis of fluorescent latex beads, and this impairment was alleviated by fucoidan treatment. In vivo, fucoidan alleviated the mechanical hyperalgesia induced by L-OHP (Fig. 4E). The effects of fucoidan on the expression of SR-A1 in the mouse intestine and DRGs were further detected. Fucoidan upregulated SR-A1 receptor expression in the intestine and DRGs (Fig. 4F and G). Moreover, fucoidan reduced the accumulation of LPS in the plasma and DRGs of CIPN mice (Fig. 4H and I) and decreased the content of HMGB1 (Fig. 4J and Figure S7), thereby inhibiting the formation of NETs and reducing H3Cit levels in the blood and DRGs (Fig. 4K and L). To further investigate the role of NETs, we performed immunohistochemical staining of DRG tissue sections using MPO (a marker for NETs) and Ly6g (a marker for neutrophils). Our results showed that L-OHP treatment significantly increased MPO-positive staining in DRG tissues, with notable co-localization with Ly6g (Figure S5), indicating enhanced NET formation. To gain further insights into NET formation, we also examined the co-localization of CitH3 and MPO in DRG tissues. Consistently, L-OHP treatment resulted in elevated levels of both CitH3 and MPO, with substantial co-localization, reinforcing the evidence of increased NET formation following L-OHP exposure (Figure S6). Notably, fucoidan treatment effectively reduced the accumulation of MPO and CitH3 in the DRG and suppressed neutrophil recruitment to this region, suggesting that fucoidan may mitigate NET accumulation and exert a potential therapeutic effect. Fucoidan also decreased the expression of TF (Fig. 4M), alleviated the disturbance of circulation in nerve endings and the intestinal tract in mice (Fig. 4N-Q), and ultimately decreased MMP9 activity (Fig. 4R). These results suggest that fucoidan might promote the clearance of LPS/HMGB1 by increasing the level of SR-A1 in phagocytic cells in the intestine and DRGs, inhibit NET formation to alleviate disturbances in circulation, and alleviate CIPN. Additionally, fucoidan prevented the increase in intestinal permeability induced by L-OHP (Fig. 4S and T). After chemotherapy, the intestinal barrier of mice was destroyed, resulting in increased leakage of LPS into the blood and increased HMGB1 production, which further damaged the intestinal barrier and resulted in positive feedback damage. Fucoidan inhibited the accumulation of LPS/HMGB1, played an indirect protective role in the intestinal tract of mice, and blocked the malignant injury cycle of the intestine–nerve axis. Additionally, the DRGs contain thousands of sensory neurons that transmit information regarding the internal and external environments to the central nervous system [36, 37]. CIPN involves neuronal apoptosis as a critical pathological mechanism [38, 39]. Platinum-based chemotherapeutics induce apoptosis by inhibiting DNA replication and transcription, while paclitaxel disrupts microtubule function and cell division, leading to apoptosis in both cancerous and healthy cells and contributing to CIPN pathogenesis [40, 41]. Building upon our previous research on the effects of fucoidan on macrophages, we investigated the effects of fucoidan on SH-SY5Y cell apoptosis in vitro. As shown in Figure S4, L-OHP increased SH-SY5Y cell apoptosis, as evidenced by increased cleaved caspase-3 expression. However, FUC had no direct therapeutic effect.

SR-A1 plays a key role in the protective effects of fucoidan via the gut–blood–DRG axis

SR-A1$^{-/-}$ mice were used to evaluate the therapeutic effect and associated parameters and to further investigate the vital role of SR-A1 in the anti-CIPN effects of fucoidan. Notably, we observed that the effects of fucoidan on LPS/HMGB1, MMP-9, and TF levels were nullified following SR-A1 knockout compared with those in the treatment group. The in vitro results confirmed that fucoidan promoted the phagocytosis of FITC-LPS and FITC-HMGB1 by BMDMs, but this effect was negated by SR-A1 knockout (Fig. 5A and B). We substituted FITC-HMGB1 with His tag-HMGB1 and analysed the expression of His tag protein via western blotting to explore the phagocytosis of His tag-HMGB1 by BMDMs. The results indicated that fucoidan increased the phagocytosis of His tag-HMGB1 by BMDMs, which was also abrogated by SR-A1 knockout (Fig. 5C). Furthermore, we observed a significant decrease in the pain threshold of the mice (Fig. 5D) in vivo, the worsening of related indices after

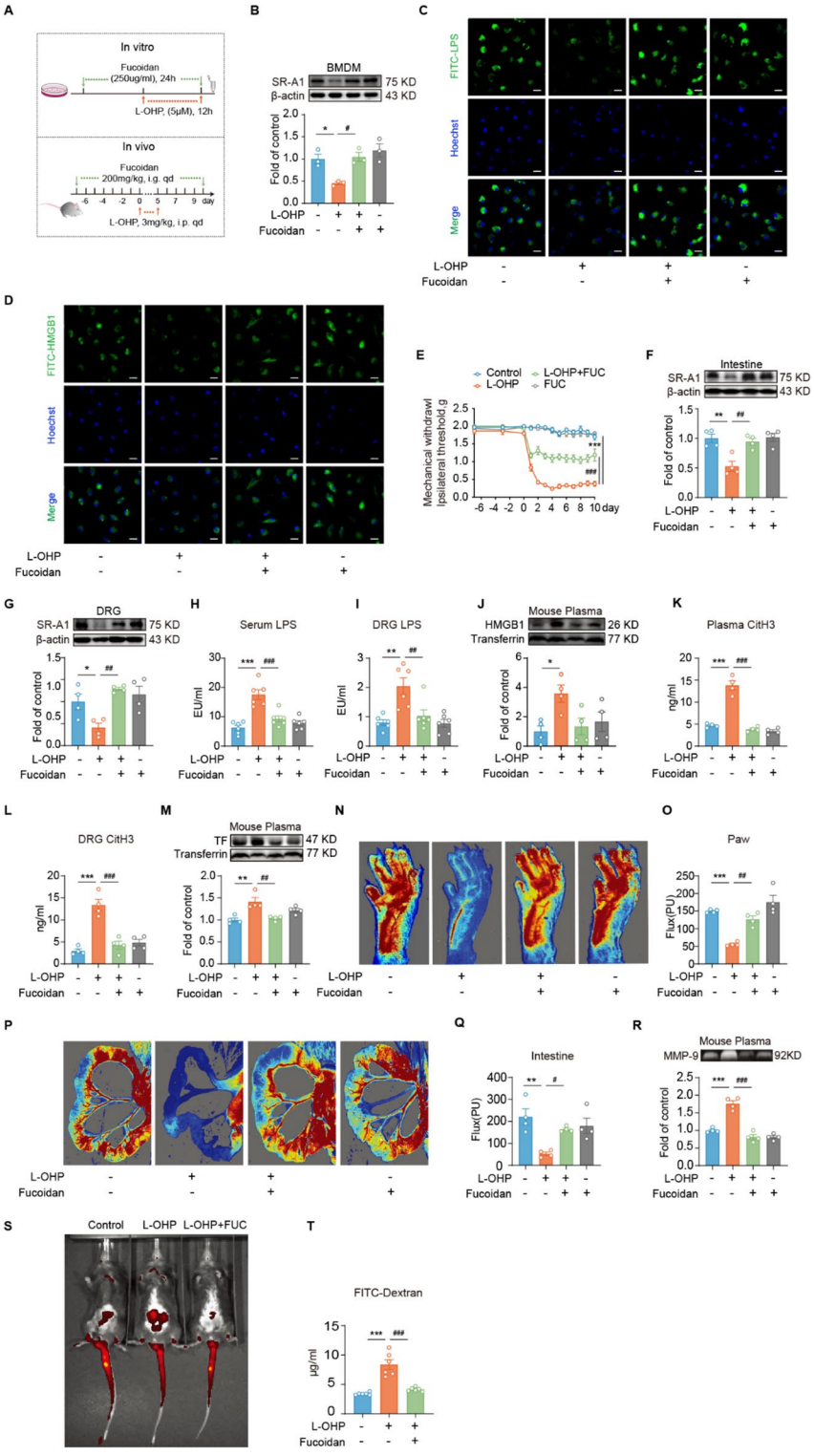

Fig. 4 (See legend on next page.)

(See figure on previous page.)

Fig. 4 Fucoidan upregulated macrophage SR-A1 expression to alleviate CIPN. (**A**) (**B**) The cells were collected, and the expression of SR-A1 was detected by western blotting ($n=3$). (**C**) (**D**) The phagocytosis of FITC-LPS and FITC-HMGB1 by BMDMs was observed under a confocal microscope ($n=3$). Scale bar: 20 μm. (**E**) A mouse CIPN model was established, and the mechanical pain threshold ($n=6$) was detected via the Von Frey test. (**F**) On the 10th day after the first injection of L-OHP, the intestinal tracts of the mice were collected to investigate the expression level of SR-A1 in the intestinal tissue by western blotting ($n=4$). (**G**) DRGs were collected from the mice to investigate the expression level of SR-A1 ($n=4$). (**H**) (**I**) The content of LPS in the serum and DRGs was detected by ELISA ($n=6$). (**J**) Mouse plasma was collected to detect HMGB1 levels ($n=4$). (**K**) (**L**) The H3Cit contents in the plasma and DRGs were detected by ELISA ($n=4$). (**M**) The levels of TF in the plasma of the mice was detected by western blotting ($n=4$). The plantar and intestinal microcirculation of the mice was measured by laser Doppler imaging ($n=4$). The differences in plantar blood flow (**N**) (**O**) and intestinal blood flow (**P**) (**Q**) between the different groups were determined ($n=4$). (**R**) The activity of MMP9 in the plasma of mice was detected by gelatine zymography ($n=4$). (**S**) FITC-dextran (600 mg/kg, i.g.) was administered on the 10th day after the first injection of L-OHP into the mice. Four hours later, the intestinal leakage of the mice was investigated by illumination with visible light in vivo. (**T**) The serum of the mice was collected, and the concentration of FITC-dextran in the serum was detected using an enzyme-labelling instrument ($n=6$). Significant differences were determined using one-way ANOVA (**B**–**M**, **O**, **Q**, **R** and **T**) or two-way ANOVA (**E**). ($^{*}p<0.05$, $^{**}p<0.01$ and $^{***}p<0.001$ compared with the control group; $^{\#}p<0.05$, $^{\#\#}p<0.01$ and $^{\#\#\#}p<0.001$ compared with the L-OHP group)

SR-A1 knockout, and increased accumulation of LPS and H3Cit in the DRGs (Fig. 5E-G). Additionally, TF expression and MMP-9 activity in the DRGs were also increased (Fig. 5H and J). We detected HIF-1α levels to assess the ischaemic status and observed that fucoidan reduced HIF-1α expression in the DRGs of CIPN mice. However, after SR-A1 knockout, the hypoxia induced by high expression of HIF-1α reappeared (Fig. 5I). Demyelination of the sciatic nerve is a significant pathological manifestation of CIPN. We observed evident increase in the demyelination of sciatic nerve in CIPN mice after chemotherapy; however, fucoidan reduced this change. Notably, this change was also nullified in SR-A1$^{-/-}$ mice (Fig. 5K). These findings revealed the critical role of SR-A1 in the process of inhibiting LPS/HMGB1/NET accumulation and decreasing MMP-9/TF/HIF-1α levels in the DRGs of CIPN mice.

Additionally, our results showed that fucoidan inhibited the excessive accumulation of LPS/HMGB1/NETs in the blood induced by L-OHP and reduced the plasma TF content and MMP-9 activity, changes that were mediated by the SR-A1 receptor (Fig. 6A-E). Fucoidan decreased the expression of TF/MMP-9 in the soles of CIPN mice after treatment, but this effect was reversed by SR-A1 knockout (Fig. 6F). We also found that the therapeutic effect of fucoidan on foot microcirculation in CINP mice relied on SR-A1, and the intestinal microcirculation results were similar (Fig. 6G). Furthermore, fucoidan indirectly protected the intestinal tract of mice by inhibiting the accumulation of PAMPs/DAMPs. As shown in Fig. 6H and I, fucoidan relieved intestinal leakage and inhibited the infiltration of macromolecular substances into the blood. The intestinal HE staining revealed that fucoidan alleviated intestinal injury in CIPN mice (Fig. 6J). Fucoidan also restored the intestinal tight junction function of CIPN mice by increasing the expression of Claudin-1 and Occludin proteins in the intestine, whereas this protective effect was abolished in SR-A1$^{-/-}$ mice (Fig. 6K and L). Overall, our findings suggested that fucoidan could reduce the accumulation of LPS/HMGB1/NETs in the blood and reduce the nerve injury induced by intestinal injury by increasing the level of SR-A1.

Fucoidan promotes the phagocytic clearance of NETs by BMDMs in an SR-A1 receptor-dependent manner

Fucoidan can inhibit the formation of NETs by promoting the phagocytic clearance of LPS/HMGB1 to alleviate CIPN. Surprisingly, we found that fucoidan could also rely on SR-A1 to phagocytose already generated NETs. As shown in Fig. 7A, compared with that in the control group, the positive rate of NET phagocytosis in the L-OHP treatment group was decreased, while fucoidan reversed this effect through the SR-A1 receptor. We further observed the dynamic process by which BMDMs phagocytose NETs using a live cell workstation, and the results revealed that BMDMs without L-OHP treatment had the ability to phagocytose NETs floating in the culture medium (Additional file 1, Movie S1). However, after L-OHP treatment, the ability of BMDMs to phagocytose NETs was reduced (Additional file 2, Movie S2). Fucoidan pretreatment improved the macrophage phagocytic function and reversed the macrophage phagocytic dysfunction caused by L-OHP (Additional file 3, Movie S3). SR-A1$^{-/-}$ mouse cells were used to further verify the relationship between fucoidan-mediated promotion of BMDM phagocytic clearance of NETs and the SR-A1 receptor. As shown in Additional file 4, Movie S4, SR-A1 knockout abolished the effect of fucoidan. Similar results were obtained when L-OHP was used to stimulate BMDMs from SR-A1$^{-/-}$ mice (Additional file 5, Movie S5). The deficiency of the SR-A1 receptor severely affected macrophage phagocytic function even without treatment (Additional file 6, Movie S6). These results indicated that fucoidan promoted macrophage phagocytosis and the clearance of NETs through the SR-A1 receptor. The mechanism of SR-A1-mediated NET-phagocytosis was further explored. Considering that SR-A1 can recognize HMGB1, an important component of NETs (Additional file 8, Figure S1), we hypothesized that the ability of SR-A1 to mediate the phagocytosis of NETs by macrophages is related to its recognition of HMGB1. We blocked the HMGB1 binding site on NETs, and Additional file 7, Movie S7 shows that the phagocytic effect of fucoidan was abolished. Hence, HMGB1 attached to NETs may serve as a recognition site

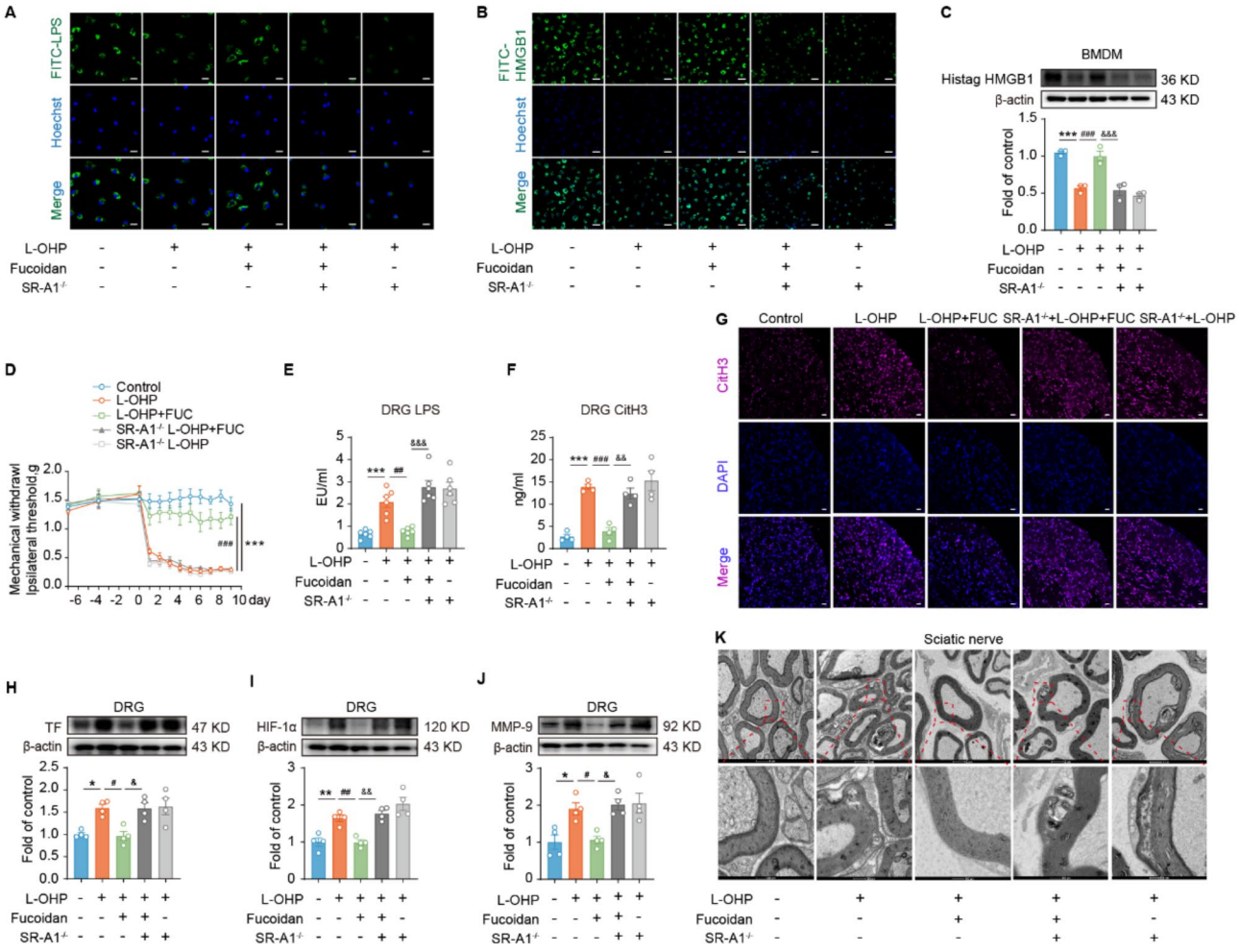

Fig. 5 SR-A1 plays a key role in the treatment of CIPN with fucoidan. (**A**) (**B**) BMDMs were obtained from SR-A1$^{-/-}$ mice and WT mice. The phagocytosis of FITC-LPS and FITC-HMGB1 by BMDMs was observed under a confocal microscope ($n=3$). (FITC-LPS: scale bar: 20 μm; FITC-HMGB1: scale bar: 40 μm). (**C**) Cellular proteins were collected, and western blotting was used to investigate the phagocytosis of His tag-HMGB1 (10 nM) by BMDMs in different groups ($n=3$). (**D**) WT mice and SR-A1$^{-/-}$ mice were administered fucoidan (200 mg/kg, I.G.) 7 days in advance, and then L-OHP (3 mg/kg, i.p.) was administered to the mice for 5 days to establish the CIPN model. The mechanical pain threshold in mice was detected using the Von Frey test ($n=6$). (**E**) (**F**) The DRGs of the mice were collected, and the contents of LPS ($n=6$) and H3Cit ($n=4$) were detected by ELISAs. (**G**) Immunofluorescence staining was performed to evaluate the expression of H3Cit in DRGs ($n=3$, scale bar: 20 μm). TF expression levels (**H**), HIF-1α protein expression levels (**I**) and MMP9 protein expression levels (**J**) in the mouse DRGs were detected by western blotting ($n=4$). (**K**) Demyelination of the sciatic nerve in response to different treatment components was investigated by transmission electron microscopy ($n=3$). Significant differences were determined using one-way ANOVA (**C**, **E**, **F**, **H**, **I** and **J**) or two-way ANOVA (**D**). ($^{*}p<0.05$, $^{**}p<0.01$ and $^{***}p<0.001$ compared with the control group; $^{\#}p<0.05$, $^{\#\#}p<0.01$ and $^{\#\#\#}p<0.001$ compared with the L-OHP group; $^{\&}p<0.05$, $^{\&\&}p<0.01$ and $^{\&\&\&}p<0.001$ compared with the L-OHP + fucoidan group)

for SR-A1, which helps fucoidan promote the phagocytic clearance of NETs by macrophages for the treatment of CIPN.

Fucoidan upregulates SR-A1 expression through the p62/Keap1/Nrf2 signaling pathway

BMDMs were collected from two groups (L-OHP and L-OHP + FUC) for RNA-seq analysis in vitro to explore the molecular mechanism by which fucoidan regulates the SR-A1 receptor. The GSVA enrichment analysis revealed a total of 41 signalling pathways related to SR-A1. Considering that LPS/HMGB1 is involved mainly in inflammation-related signals during CIPN, we analysed these SR-A1-related pathways from the point of view of inflammatory signals and selected inflammatory signalling pathways for analysis (Fig. 7B). The "NEMETH_INFLAMMATORY_RESPONSE_LPS_UP" signalling pathway involves 87 genes, among which 9 were significantly differentially expressed (Fig. 7C), and the names of these genes are shown in Fig. 7D. Among these 9 genes, the Sqstm1 (p62) gene is located on chromosome 5 and is a multifunctional protein that regulates the NF-κB signalling pathway [42, 43]. Furthermore, Sqstm1 can regulate the expression of SR-A1 [44]. Therefore, sqstm1

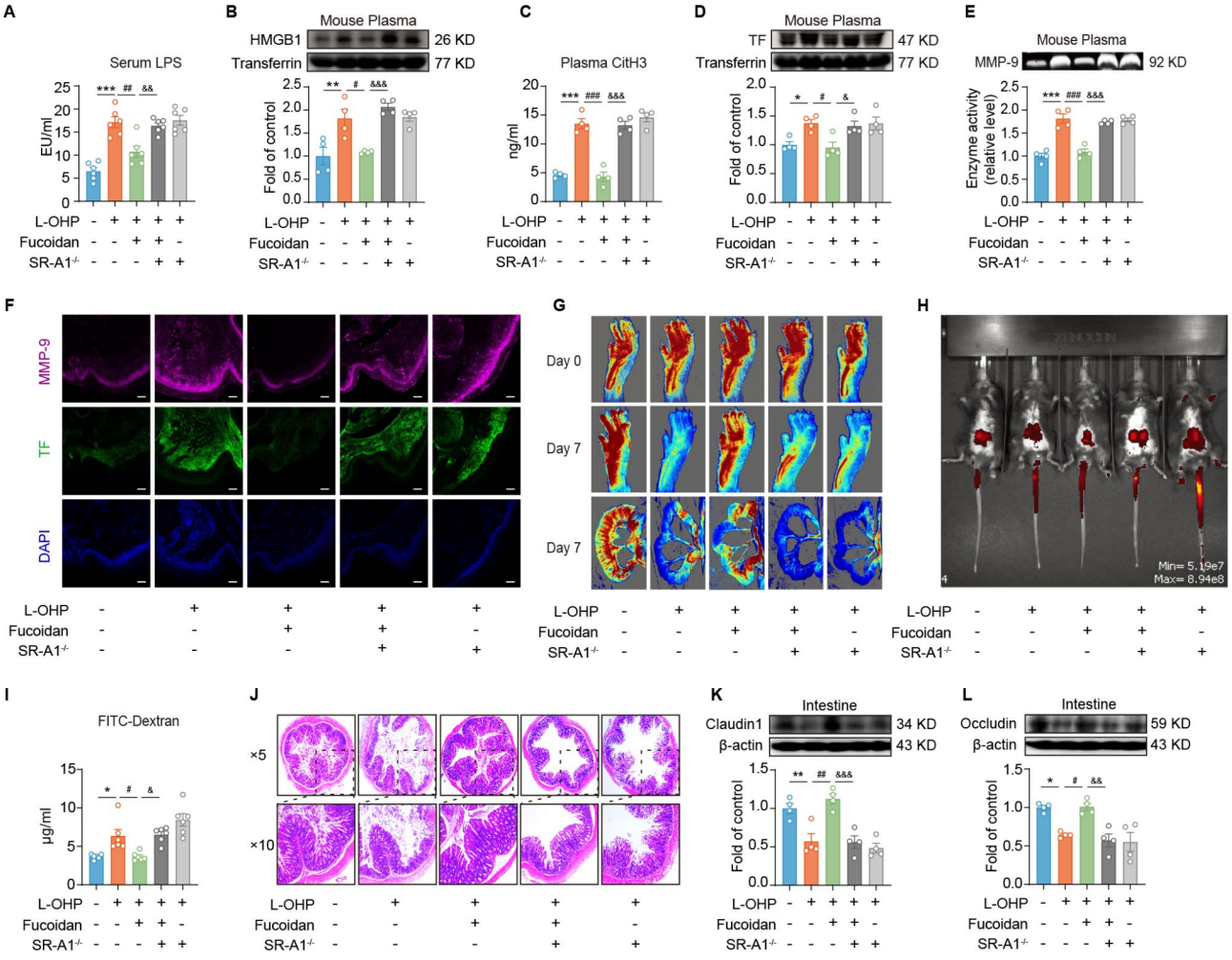

Fig. 6 SR-A1 plays a key role in the treatment of CIPN with fucoidan. (**A**) The serum of the mice was collected to detect the LPS content via ELISA ($n=6$). (**B**) (**C**) Plasma was collected to detect the levels of HMGB1 ($n=4$) and H3Cit ($n=4$). (**D**) TF expression and MMP9 activity (**E**) were investigated ($n=4$). (**F**) The TF/MMP9 ratio in the feet of the mice was qualitatively investigated by immunofluorescence staining ($n=3$). Scale bar: 50 μm. (**G**) Laser Doppler imaging was used to investigate the microcirculatory status of the plantar surface and intestinal tracts in mice ($n=4$). (**H**) FITC-dextran was administered to the mice for four hours, and intestinal leakage was investigated by illumination with visible light. (**I**) The serum of the mice was collected, and the concentration of FITC-dextran was detected using an enzyme labelling instrument ($n=6$). (**J**) The intestines of the mice were collected, fixed with 4% paraformaldehyde, and stained with HE ($n=3$). Claudin-1 protein (**K**) and Occludin protein (**L**) levels in the intestinal tract of the mice were detected via western blotting ($n=4$). Significant differences were determined using one-way ANOVA (A-C, E, F, J, L and M). ($^{*}p<0.05$, $^{**}p<0.01$ and $^{***}p<0.001$ compared with the control group; $^{\#}p<0.05$, $^{\#\#}p<0.01$ and $^{\#\#\#}p<0.001$ compared with the L-OHP group; $^{\&}p<0.05$, $^{\&\&}p<0.01$ and $^{\&\&\&}p<0.001$ compared with the L-OHP + fucoidan group)

was used to explore the target by which fucoidan regulates SR-A1 (Fig. 7D). Studies have shown that p62 helps Nrf2 escape into the nucleus through competitive binding to Keap1 and ultimately regulates the expression of the SR-A1 receptor [44]. We confirmed that the expression of p62 in BMDMs decreased after L-OHP stimulation and that p62 expression increased after treatment with fucoidan (Fig. 7E). We further detected the Nrf2 protein level in the nucleus. As shown in Fig. 7F, the expression of Nrf2 in the nucleus of BMDMs decreased after L-OHP stimulation. Fucoidan increased the Nrf2 protein level. The co-IP results revealed that the binding of p62 to Keap1 decreased and that the binding of Nrf2 to Keap1 increased after L-OHP stimulation, whereas after treatment with fucoidan, p62 competed to bind Keap1, which significantly increased Nrf2 nuclear translocation (Fig. 7G). These results suggest that fucoidan promotes p62 to compete with Keap1 for binding to Nrf2, releases Nrf2 into the nucleus, and then regulates SR-A1 transcription. ML385, an inhibitor of Nrf2, was used to confirm the upregulation of SR-A1 by fucoidan at the transcriptional level, and the translation of SR-A1 was reversed (Fig. 7H and I). These results revealed that fucoidan acted on the SR-A1 receptor through the p62/Keap1/Nrf2 signalling pathway.

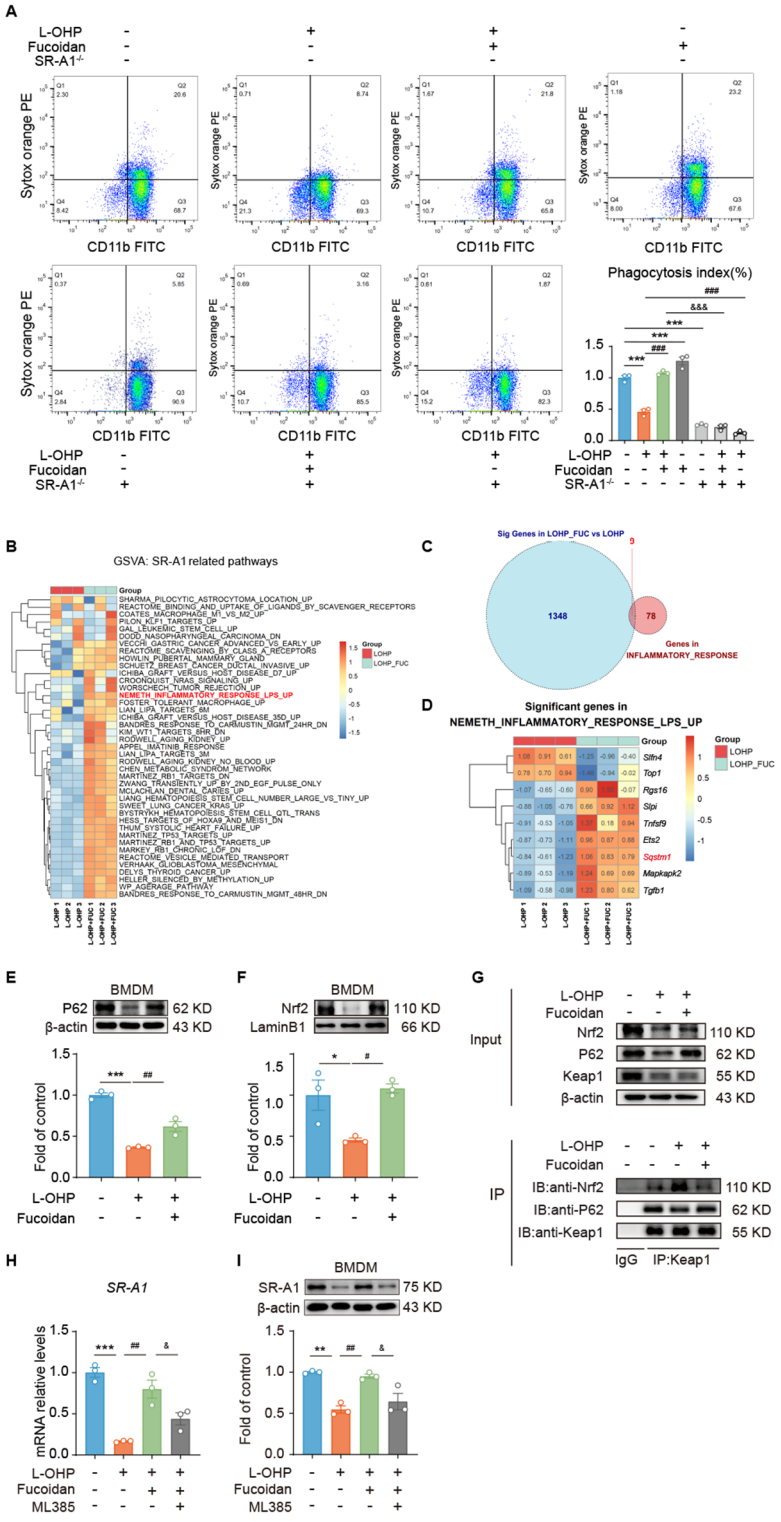

Fig. 7 (See legend on next page.)

(See figure on previous page.)

Fig. 7 Fucoidan upregulates SR-A1 expression through the p62/Keap1/Nrf2 signalling pathway. (**A**) BMDMs were obtained from SR-A1$^{-/-}$ mice and WT mice. Fucoidan (250 μg/ml) was added to prestimulate the cells for 12 h, and then L-OHP (5 μM) was added and incubated for 12 h. NETs marked with SYTOX orange (500 ng/ml) were added, and the phagocytosis of NETs by BMDMs was detected using flow cytometry ($n = 3$). (**B**) BMDMs were obtained from WT mice, pretreated with fucoidan (250 μg/ml) for 12 h, and then stimulated with L-OHP (5 μM) for 12 h. The cells were collected for RNA-seq. SR-A1-related pathways were subjected to GSVA enrichment analysis. (**C**) (**D**) A total of 1357 genes were significantly different between the L-OHP group and the L-OHP + FUC group. Eighty-seven genes were involved in the "NEMETH_INFLAMMATORY_RESPONSE_LPS_UP" signalling pathway, 9 of which were significantly differentially expressed ($n = 3$). (**E**) The proteins were collected from cells stimulated with L-OHP (5 μM) for 18 h, and the expression of the p62 protein was detected by western blotting ($n = 3$). (**F**) Nuclear protein was collected, and Nrf2 protein levels were detected by western blotting ($n = 3$). (**G**) Cellular proteins were collected, and co-IP was used to verify the relationships among p62/Keap1/Nrf2. (**H**) BMDMs were pretreated with the Nrf2 inhibitor ML385 (10 μM), stimulated with fucoidan (250 μg/ml) for 12 h, and then stimulated with L-OHP (5 μM) for 18 h. Cells were collected, and qPCR was performed to detect the SR-A1 mRNA level ($n = 3$). (**I**) The SR-A1 protein expression level was detected via western blotting ($n = 3$). Significant differences were determined using one-way ANOVA (**D**-**G** and **H**). ($^{*}p < 0.05$, $^{**}p < 0.01$ and $^{***}p < 0.001$ compared with the control group; $^{\#}p < 0.05$, $^{\#\#}p < 0.01$ and $^{\#\#\#}p < 0.001$ compared with the L-OHP group; $^{\&}p < 0.05$, $^{\&\&}p < 0.01$ and $^{\&\&\&}p < 0.001$ compared with the L-OHP + fucoidan group)

Fucoidan regulates the gut microbiota and attenuates the progression of CIPN

Fucoidan affects the p62/Keap1/Nrf2 signalling axis to promote macrophage phagocytosis and the clearance of LPS. LPS is derived from gut bacteria and is a key component of the outer membrane of gram-negative bacteria [45]. Mouse faeces were collected for a sequencing analysis (16 S) of microbial diversity to explore the possible source of LPS. The results shown in Fig. 8A indicate that, compared with L-OHP, fucoidan increased the abundance and diversity of the gut microbiota in mice. PLS-DA was performed to explore the beta diversity of the gut microbiota across different treatment groups, revealing a marked separation in the overall species composition between the L-OHP group and the fucoidan group (Fig. 8B). The results of the rank abundance curve analysis revealed that L-OHP strongly decreased the abundance of the gut microbiota, whereas fucoidan increased the species abundance (Fig. 8C), suggesting that fucoidan has a protective effect on the abundance of the gut microbiota. At the phylum level, the plot of the taxonomic classification of the top 20 ranked phyla revealed that, compared with those in the control group, the relative abundance of Bacteroidetes decreased and that of Firmicutes increased in the L-OHP group, resulting in a decreased Bacteroidetes/Firmicutes ratio. The abundance of Verrucomicrobia also decreased. Fucoidan increased the abundances of Bacteroidetes and Verrucomicrobia and decreased the abundance of Firmicutes, leading to an increase in the Bacteroidetes/Firmicutes ratio (Fig. 8D). The results of the star analysis indicated that the predominant microbial groups in the top 10 ranked phyla of the L-OHP group were Actinobacteria and Firmicutes. In the fucoidan treatment group, the dominant microbial groups were Bacteroidetes and Verrucomicrobia, whereas the abundance of Actinobacteria was significantly decreased (Fig. 8E), indicating that fucoidan could exert neuroprotective effects by regulating the gut microbiota.

Furthermore, linear discriminant analysis effect size (LEfSe) revealed that the abundances of the c_Bacilli, f_Bacteroidacea and g_Bacteroides taxa in the control group (blue) were different from those in the other groups. As shown in Fig. 8K, the L-OHP group (red) was significantly different from the other groups in terms of p_Firmicutes and f_Lactobacillaceae abundances. The fucoidan treatment group (green) presented notable increases in g_Muribaculaceae and f_Muribaculaceae abundances, whereas the group treated with fucoidan alone (grey) presented significant increases in o_Bacteroidales, p_Bacteroidota, and c_Bacteroidia abundances (Fig. 8F and G). We created a clustering heatmap of the top 20 genera in the four groups to further elucidate the changes in the gut microbiota composition (Fig. 8H). Compared with L-OHP, fucoidan increased the abundances of Muribaculaceae, Alistipes, and Akkermansia but decreased the abundances of Turicibacter, Clostridium, Lactobacillus, and Parabacteroides in mouse faeces. Interestingly, as shown by the results of the bugBase analysis, L-OHP caused a decrease in the abundance of gram-negative bacteria and an increase in the abundance of gram-positive bacteria (Fig. 8I and J). Further analysis revealed that after L-OHP stimulation, the abundance of Bacteroidetes was decreased among gram-negative bacteria, whereas the relative abundance of Verrucomicrobia was slightly decreased. Among the gram-positive bacteria, the abundance of Firmicutes increased. Conversely, in the fucoidan group, the relative abundance of Bacteroidetes was increased, whereas the abundance of Firmicutes decreased (Fig. 8K and L). Studies have shown that Bacteroidetes can migrate through a unique gliding motility and type IX secretion system (T9SS) [46], and gram-negative bacteria incubated with plasma can release a significant amount of LPS. This result suggested that after the L-OHP-induced disruption of the intestinal mucosal barrier, large numbers of Bacteroidetes might migrate into the bloodstream and release LPS, which could be a critical factor contributing to the excessive accumulation of LPS in the bloodstream and DRGs. Therefore, we suggest that fucoidan protects the intestinal mucosal barrier, maintains gut microbiota stability, suppresses the massive migration of Bacteroidetes into the bloodstream, reduces the accumulation of LPS in

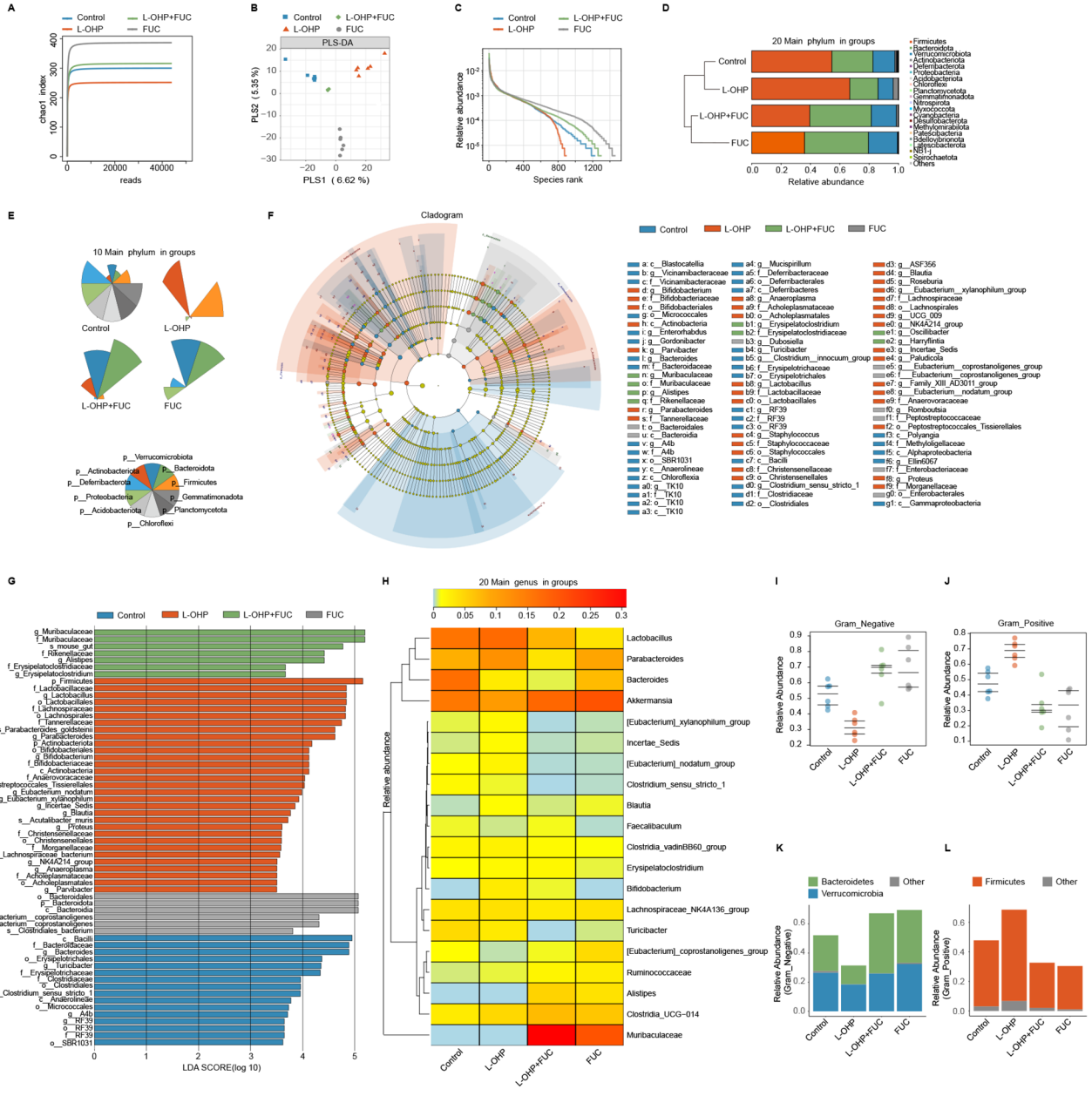

Fig. 8 Fucoidan regulates the gut microbiota and alleviates CIPN by affecting the gut–nerve axis. (**A**) The Chao1 index was used to estimate the diversity of the gut microbiota. (**B**) Partial least squares-discriminant analysis (PLS-DA) was performed to analyse the beta diversity of the intestinal microbiota in the faeces from the four groups of mice. (**C**) Rank abundance curves were constructed to analyse the richness and evenness of species in the samples. (**D**) Clustering heatmap analysis of faecal phylum-level species showing the changes in the relative abundances in the top 20 phylum-level species in the faeces from the four groups of mice. (**E**) Phylum-level star analysis showing the changes in the relative abundances of the top 10 phyla in the faeces from the four groups of mice. (**F**) Linear discriminant analysis effect size (LEfSe) was used to display the evolutionary relationship of the entire species system, the distribution patterns of important species in different groups, and the distribution of the abundances of species with significant differences between groups (the LDA threshold was 3), as well as to identify the species with significant differences in the intestinal microbiota among all classification levels in the faeces from the four groups of mice. (**G**) The LDA threshold was 3.5. (**H**) Clustering heatmap analysis of the changes in the relative abundances of the top 20 genera in the faeces from the four groups of mice. (**I**) (**J**) An inter-group analysis of differences in phenotypic abundances can intuitively reflect the median, dispersion, maximum value, minimum value, and outliers of species diversity within each group. (**K**) (**L**) Phenotypic abundance reflects the relative abundance percentage of a species

the bloodstream and DRGs, and ultimately contributes to the treatment of CIPN.

Discussion

In this study, we found that excessive amounts of LPS/HMGB1/NETs accumulated in the blood of patients and animals. Insufficient clearance of LPS/HMGB1 by macrophages is a major cause of excessive NET formation. L-OHP inhibited SR-A1 expression, contributing to the insufficient phagocytosis by macrophages. Fucoidan could upregulate SR-A1 expression, promote macrophage phagocytosis of LPS/HMGB1, decrease NET contents in mouse plasma and DRGs, and alleviate microcirculation disorders induced by NETs. SR-A1 knockout abolished the protective effect of fucoidan. Surprisingly, we found that fucoidan promoted macrophage phagocytosis of NETs, which depended on the recognition of the interaction between SR-A1 and HMGB1, since HMGB1 is a component of NETs. The RNA-seq analysis revealed that, compared with L-OHP, fucoidan significantly upregulated the expression of the p62 gene. Fucoidan increased SR-A1 expression through the P62/Keap1/Nrf2 axis. Finally, fucoidan maintained the diversity of the gut microbiota, increased the abundance of Bacteroidetes, and decreased the abundances of Firmicutes and Actinobacteria compared with those in the L-OHP group.

Our previous research reported that NETs play an important role in the process of CIPN [9, 10]. Here, we focused on how to inhibit NET formation and solve this problem at the source. Since LPS/HMGB1 are important factors triggering NET formation, we analysed the correlation between LPS/HMGB1/NETs and CIPN. As shown in Figs. 1 and 2 and a significant accumulation of LPS/HMGB1/NETs was observed in the plasma of both CIPN patients and mice. LPS is a distinct constituent of the cell wall in gram-negative bacteria [45], and it appears to accumulate excessively in both the blood and DRGs, potentially originating from gram-negative bacteria in the intestine. Research has shown that increased levels of LPS leakage from the gut microbiota into the bloodstream exacerbate oxaliplatin-induced mechanical pain hypersensitivity via the TLR4 pathway [16], which is consistent with our data showing that LPS accumulates in mouse serum. A previous study showed that the levels of LPS are notably elevated in the colon, serum, and SN of Parkinson's disease (PD) models and that gut dysbiosis induced by fisetin is involved in the pathogenesis of PD through the microbiota–gut–brain axis [47]. After chemotherapy, a large amount of HMGB1 is released from LPS-stimulated or apoptotic cells [19, 48]. Therefore, the excessive accumulation of LPS/HMGB1 in the blood and DRGs induces the formation of NETs, resulting in microcirculatory disorders and causing CIPN.

We further investigated the reasons for the accumulation of LPS/HMGB1 by measuring the mRNA levels of receptors expressed on the macrophage membrane that can bind to LPS/HMGB1. We found that insufficient expression of the macrophage scavenging receptor SR-A1 caused by chemotherapy was an important reason for the accumulation of LPS/HMGB1 (Fig. 3). These data are similar to those of a previous study in which SR-A1 was shown to mediate the clearance of plasma endotoxin [49]. Furthermore, fucoidan upregulated SR-A1 expression, promoted the phagocytosis of LPS/HMGB1 by macrophages, and subsequently inhibited NET formation and microcirculation disorders, alleviating CIPN (Fig. 4). The protective effects of fucoidan were abolished by SR-A1 knockout (Figs. 5 and 6). Interestingly, fucoidan not only reduced the accumulation of LPS/HMGB1 and inhibited the formation of NETs but also had a direct effect on the phagocytosis of NETs that had already been generated during chemotherapy, which was also dependent on the SR-A1 receptor (Additional files 1–6, Movies S1–6). These results indicate that SR-A1 participates in the phagocytic function of macrophages and mediates the engulfment of large molecules.

Some studies have shown that SR-A1 can interact with Tyro3 receptors, promote macrophages to phagocytose and clear apoptotic cells (ACs) and alleviate acute aortic dissection [50]. Another report suggested that SR-A is essential for the optimal phosphorylation of MerTK and the subsequent signalling required for AC uptake, which inhibits inflammation and infection [51]. These studies provide potential strategies for the SR-A1-mediated phagocytosis of NETs by macrophages. A previous study reported that HMGB1 is a major component of NETs [52, 53], which is consistent with our data (as shown in Figure S1) indicating that SYTOX orange-labelled NETs were colocalized with FITC-labelled HMGB1, suggesting the presence of substantial amounts of HMGB1 within the NETs. Furthermore, we found that blocking HMGB1 with an anti-HMGB1 antibody inhibited the phagocytosis of NETs by macrophages (Additional file 7, Movie S7). Therefore, SR-A1 may recognize and phagocytose NETs by binding to HMGB1 within NETs.

We performed gene sequencing and explored GSVA enrichment data related to the SR-A1 pathway to investigate the mechanism by which fucoidan upregulates SR-A1. The results revealed that the p62 gene was significantly upregulated after fucoidan treatment. p62 competes with Nrf2 for binding to Keap1, promoting Nrf2 escape into the nucleus and regulating the transcription of SR-A1. Therefore, the p62/Keap1/Nrf2 signalling pathway may be one of the important mechanisms by which fucoidan regulates SR-A1 expression. However, there are limitations in our study. The specific molecular mechanisms by which fucoidan modulate p62 expression, particularly the identification of the target molecule(s) directly interacting with p62 to promote its upregulation, have not been fully elucidated

and require additional research. Elucidation of this target is crucial for the rationale design and development of novel small-molecule therapeutic agents, which may provide an effective clinical strategy to address the significant challenge of CIPN, for which currently there are limited effective treatment options.

Our research revealed that the accumulation of LPS, which is a crucial factor contributing to the formation of NETs, in the bloodstream was caused primarily by damage to the intestinal mucosal barrier and increased intestinal permeability. Since LPS is present mainly on the surface of gram-negative bacteria in the intestine [45, 54], we conducted further investigations of the impact of fucoidan on the intestinal microbiota (Fig. 8). We observed a significant decrease in the abundance of the Bacteroidetes phylum of gram-negative bacteria in mouse faeces after L-OHP stimulation. Conversely, fucoidan significantly increased the abundance of Bacteroides. Previous studies have shown that, compared with the Firmicutes phylum, the Bacteroidetes phylum has greater mobility due to the presence of unique cell surface adhesins that facilitate gliding motility and an IX secretion system that promotes translocation, resulting in a higher migration rate [55, 56]. Additionally, a high-pressure model of the peritoneal cavity leads to increased intestinal permeability and gut microbiota disruption, as evidenced by the migration of Bacteroides from the colon to the ileum [57]. We speculate that after L-OHP stimulation, the intestinal barrier is disrupted, facilitating the entry of highly mobile gram-negative bacteria, such as those belonging to the Bacteroidetes phylum, into the bloodstream, leading to a significant reduction in the abundance of Bacteroides in the mouse gut. The detection of LPS in the blood (Fig. 2J) corroborated our hypothesis that many gram-negative bacteria entered the bloodstream after chemotherapy.

Additionally, fucoidan is a complex polysaccharide derived from brown algae and some marine invertebrates and is mainly composed of L-fucose and sulfate ester groups [58, 59]. It can be degraded and metabolized into fucose, and research has shown that the intestine itself can perform fucosylation. Fucose is metabolized by intestinal microbes, which affects the activity of microbial metabolic pathways and reduces the expression of bacterial virulence genes [29]. Fucosylated proteins are released into the lumen, inhibiting the invasion of harmful pathogens such as *Salmonella typhi* and providing protection against pathogen infection, thereby maintaining intestinal microbial stability [60]. However, when intestinal epithelial fucosylation is lacking, intestinal inflammation worsens [61]. Our study revealed that L-OHP reduced the abundance of Bacteroides, whereas fucoidan increased the abundance of Bacteroides (Fig. 8). Intestinal epithelial fucosylation can be induced and utilized by Bacteroides [62]. Like mammals, Bacteroides modify its capsule polysaccharides and glycoproteins through a salvage metabolic pathway. This process is crucial for bacterial colonization and symbiosis with the host. Bacteroides can also produce various fucosidases that remove fucose from host glycans to achieve high fucose availability in the gut lumen [63]. Numerous studies have shown that during enteritis, the ratio of Bacteroides to Firmicutes decreases [64], and we have verified this finding. L-OHP reduces the abundance of Bacteroides and increases the abundance of Firmicutes, whereas fucoidan reverses these changes. These results suggest that fucoidan increases the abundance of Bacteroides, enhances the cleavage and utilization of fucose by the intestinal microbiota, provides energy for the intestinal microbiota, and maintains the intestinal microbial diversity and abundance, thereby maintaining intestinal microbial stability. Finally, by directly supplementing exogenous fucose, fucoidan promotes intestinal epithelial fucosylation to resist the invasion of harmful intestinal bacteria, ultimately protecting the intestine.

In conclusion, fucoidan upregulates SR-A1 expression through the p62/Keap1/Nrf2 signaling pathway to promote macrophage phagocytosis of HMGB1/LPS/NETs and maintains gut microbial homeostasis, alleviating CIPN (Graphical Abstract). This study may provide new ideas and potential therapeutic approaches for the treatment of CIPN.

Abbreviations

CIPN	Chemotherapy-induced peripheral neuropathy
SR-A1	Scavenger receptor A1
BMDM	Bone marrow-derived macrophage
HMGB1	High mobility group protein B1
LPS	Lipopolysaccharide
NETs	Neutrophil extracellular traps
DRG	Dorsal Root Ganglion
H3Cit	Histone H3
TF	Tissue Factor
MMP9	Matrix Metalloproteinase 9
L-OHP	Oxaliplatin
FUC	Fucoidan

Supplementary Information

The online version contains supplementary material available at https://doi.org/10.1186/s12974-025-03431-5.

Supplementary Material 1

Supplementary Material 2

Supplementary Material 3

Supplementary Material 4

Supplementary Material 5

Supplementary Material 6

Supplementary Material 7

Supplementary Material 8

Supplementary Material 9

Supplementary Material 10

Supplementary Material 11

Supplementary Material 12

Supplementary Material 13

Supplementary Material 14

Supplementary Material 15

Supplementary Material 16

Supplementary Material 17

Acknowledgements
Not applicable.

Author contributions
W-TL, LH and J-XM designed the project, conducted experiments, processed data, interpreted results, and edited the manuscript. R-MJ, LW, LJ conducted experiments, processed data, and interpreted results. Q-YT, Y-YC, M-YZ, LJ, Y-JZ, XZ, CM, Y-HC and R-MJ designed experiments, interpreted results, and wrote and edited the manuscript. W-TL, LH, J-XM, XZ, X-FW and Y-YC procured funding, designed experiments, and wrote and edited the manuscript.

Funding
This work was supported by the National Natural Science Foundation of China (grant number: 82271252, 81971047) and Basic Research Project of Changzhou Medical Center of Nanjing Medical University (grant number: CMCB202408) for Wentao Liu; National Natural Science Foundation of China (grant number: 82204542) for Liang Hu; National Natural Science Foundation of China (grant number: 82073910) for Xuefeng Wu; the Lianyungang Science and Technology Program Project (grant number: SF2122) for Xia Zhu; the Science and Technology Projects of Lianyungang (Social Development) (grant number: SF2314) and the Jiangsu Provincial Administration of Traditional Chinese Medicine (grant number: MS2023122) for Jianxin Ma; and the Pioneer Incubator Fund (grant number: GWRX-BR-2024-3) for Yongyi Chen.

Data availability
The RNA sequencing data sets presented in this study have been deposited in the NCBI Gene Expression Omnibus database at https://www.ncbi.nlm.nih.gov/, reference number GEO GSE249275. All data generated and analyzed during this study are included in this published article and its additional information.

Declarations

Ethics approval and consent to participate
The study was reviewed and approved by the Nanjing First Hospital Institutional Review Committee with ethics number KY20171228-KS-01. All experimental methods were conducted in accordance with relevant guidelines and regulations. The experimental plan involving animals was approved by the Committee of Experimental Animal Ethics of Nanjing Medical University through the "Examination of Ethical Welfare of Experimental Animals" and complies with relevant national welfare ethics provisions for experimental animals. The approval number is IACUC-2011040.

Consent for publication
Not applicable.

Competing interests
The authors declare no competing interests.

Author details
[1]Department of Pharmacology, School of Basic Medical Sciences, Nanjing Medical University, Nanjing 211166, Jiangsu, China
[2]State Key Laboratory of Pharmaceutical Biotechnology, School of Life Sciences, Nanjing University, Nanjing, Jiangsu 210023, China
[3]Central Laboratory, Department of Biobank, Nanjing Hospital of Chinese Medicine, Nanjing University of Chinese Medicine, Nanjing, Jiangsu 210022, China
[4]Department of Oncology, Lianyungang Municipal Oriental Hospital, Lianyungang, Jiangsu 222042, China
[5]Department of Anesthesiology, The Affiliated Cancer Hospital of Nanjing Medical University & Jiangsu Cancer Hospital & Jiangsu Institute of Cancer Research, Nanjing, Jiangsu 210009, China
[6]Department of Pathology, The First Affiliated Hospital of Nanjing Medical University, Nanjing, Jiangsu, China

Received: 23 October 2024 / Accepted: 26 March 2025
Published online: 04 April 2025

References

1. Brown TJ, Sedhom R, Gupta A. Chemotherapy-Induced peripheral neuropathy. JAMA Oncol. 2019;5:750.
2. Battaglini E, Goldstein D, Grimison P, McCullough S, Mendoza-Jones P, Park SB. Chemotherapy-Induced peripheral neurotoxicity in cancer survivors: predictors of Long-Term patient outcomes. J Natl Compr Canc Netw. 2021;19:821–8.
3. Loprinzi CL, Lacchetti C, Bleeker J, Cavaletti G, Chauhan C, Hertz DL, Kelley MR, Lavino A, Lustberg MB, Paice JA, et al. Prevention and management of Chemotherapy-Induced peripheral neuropathy in survivors of adult cancers: ASCO guideline update. J Clin Oncol. 2020;38:3325–48.
4. Hertz DL, Childs DS, Park SB, Faithfull S, Ke Y, Ali NT, McGlown SM, Chan A, Grech LB, Loprinzi CL, et al. Patient-centric decision framework for treatment alterations in patients with Chemotherapy-induced peripheral neuropathy (CIPN). Cancer Treat Rev. 2021;99:102241.
5. Lee KH, Kronbichler A, Park DD, Park Y, Moon H, Kim H, Choi JH, Choi Y, Shim S, Lyu IS, et al. Neutrophil extracellular traps (NETs) in autoimmune diseases: A comprehensive review. Autoimmun Rev. 2017;16:1160–73.
6. Zhang R, Sun C, Han Y, Huang L, Sheng H, Wang J, Zhang Y, Lai J, Yuan J, Chen X, et al. Neutrophil autophagy and NETosis in COVID-19: perspectives. Autophagy. 2023;19:758–67.
7. Middleton EA, He XY, Denorme F, Campbell RA, Ng D, Salvatore SP, Mostyka M, Baxter-Stoltzfus A, Borczuk AC, Loda M, et al. Neutrophil extracellular traps contribute to immunothrombosis in COVID-19 acute respiratory distress syndrome. Blood. 2020;136:1169–79.
8. Caxaria S, Bharde S, Fuller AM, Evans R, Thomas B, Celik P, Dell'Accio F, Yona S, Gilroy D, Voisin MB, et al. Neutrophils infiltrate sensory ganglia and mediate chronic widespread pain in fibromyalgia. Proc Natl Acad Sci U S A. 2023;120:e2211631120.
9. Lin T, Hu L, Hu F, Li K, Wang CY, Zong LJ, Zhao YQ, Zhang X, Li Y, Yang Y, et al. NET-Triggered NLRP3 activation and IL18 release drive Oxaliplatin-Induced peripheral neuropathy. Cancer Immunol Res. 2022;10:1542–58.
10. Wang CY, Lin TT, Hu L, Xu CJ, Hu F, Wan L, Yang X, Wu XF, Zhang XT, Li Y, et al. Neutrophil extracellular traps as a unique target in the treatment of chemotherapy-induced peripheral neuropathy. EBioMedicine. 2023;90:104499.
11. Papayannopoulos V. Neutrophil extracellular traps in immunity and disease. Nat Rev Immunol. 2018;18:134–47.
12. Bukong TN, Cho Y, Iracheta-Vellve A, Saha B, Lowe P, Adejumo A, Furi I, Ambade A, Gyongyosi B, Catalano D, et al. Abnormal neutrophil traps and impaired efferocytosis contribute to liver injury and sepsis severity after binge alcohol use. J Hepatol. 2018;69:1145–54.
13. Li J, Xia Y, Sun B, Zheng N, Li Y, Pang X, Yang F, Zhao X, Ji Z, Yu H, et al. Neutrophil extracellular traps induced by the hypoxic microenvironment in gastric cancer augment tumour growth. Cell Commun Signal. 2023;21:86.
14. Shinde-Jadhav S, Mansure JJ, Rayes RF, Marcq G, Ayoub M, Skowronski R, Kool R, Bourdeau F, Brimo F, Spicer J, Kassouf W. Role of neutrophil extracellular traps in radiation resistance of invasive bladder cancer. Nat Commun. 2021;12:2776.
15. Fiore NT, Debs SR, Hayes JP, Duffy SS, Moalem-Taylor G. Pain-resolving immune mechanisms in neuropathic pain. Nat Rev Neurol 2023;19(4):199–220.
16. Shen S, Lim G, You Z, Ding W, Huang P, Ran C, Doheny J, Caravan P, Tate S, Hu K, et al. Gut microbiota is critical for the induction of chemotherapy-induced pain. Nat Neurosci. 2017;20:1213–6.
17. Zhang H, Li Y, de Carvalho-Barbosa M, Kavelaars A, Heijnen CJ, Albrecht PJ, Dougherty PM. Dorsal root ganglion infiltration by macrophages contributes to Paclitaxel Chemotherapy-Induced peripheral neuropathy. J Pain. 2016;17:775–86.
18. Du Y, Xu CL, Yu J, Liu K, Lin SD, Hu TT, Qu FH, Guo F, Lou GD, Nishibori M, et al. HMGB1 in the mPFC governs comorbid anxiety in neuropathic pain. J Headache Pain. 2022;23:102.

19. Yang X, Jia R, Hu F, Fan W, Lin T, Zhang X, Xu C, Ruan S, Jiang C, Li Y, et al. Promoting AMPK/SR-A1-mediated clearance of HMGB1 attenuates chemotherapy-induced peripheral neuropathy. Cell Commun Signal. 2023;21:99.
20. Tsubota M, Fukuda R, Hayashi Y, Miyazaki T, Ueda S, Yamashita R, Koike N, Sekiguchi F, Wake H, Wakatsuki S, et al. Role of non-macrophage cell-derived HMGB1 in oxaliplatin-induced peripheral neuropathy and its prevention by the thrombin/thrombomodulin system in rodents: negative impact of anticoagulants. J Neuroinflammation. 2019;16:199.
21. Gu H, Wang C, Li J, Yang Y, Sun W, Jiang C, Li Y, Ni M, Liu WT, Cheng Z, Hu L. High mobility group box-1-toll-like receptor 4-phosphatidylinositol 3-kinase/protein kinase B-mediated generation of matrix metalloproteinase-9 in the dorsal root ganglion promotes chemotherapy-induced peripheral neuropathy. Int J Cancer. 2020;146:2810–21.
22. Araldi D, Khomula EV, Bonet IJM, Bogen O, Green PG, Levine JD. Role of pattern recognition receptors in chemotherapy-induced neuropathic pain. Brain 2024;147(3):1025–1042.
23. Cabral F, Al-Rahem M, Skaggs J, Thomas TA, Kumar N, Wu Q, Fadda P, Yu L, Robinson JM, Kim J, et al. Stabilin receptors clear LPS and control systemic inflammation. iScience. 2021;24:103337.
24. Xu J, Jiang Y, Wang J, Shi X, Liu Q, Liu Z, Li Y, Scott MJ, Xiao G, Li S, et al. Macrophage endocytosis of high-mobility group box 1 triggers pyroptosis. Cell Death Differ. 2014;21:1229–39.
25. Zani IA, Stephen SL, Mughal NA, Russell D, Homer-Vanniasinkam S, Wheatcroft SB, Ponnambalam S. Scavenger receptor structure and function in health and disease. Cells. 2015;4:178–201.
26. Zhu X, Wang Y, Zhu L, Zhu Y, Zhang K, Wang L, Bai H, Yang Q, Ben J, Zhang H, et al. Class A1 scavenger receptor prevents obesity-associated blood pressure elevation through suppressing overproduction of vascular endothelial growth factor B in macrophages. Cardiovasc Res. 2021;117:547–60.
27. Wang Y, Xing M, Cao Q, Ji A, Liang H, Song S. Biological activities of fucoidan and the factors mediating its therapeutic effects: A review of recent studies. Mar Drugs. 2019;17(3):183.
28. Yao Y, Zaw AM, Anderson DEJ, Hinds MT, Yim EKF. Fucoidan functionalization on poly(vinyl alcohol) hydrogels for improved endothelialization and hemocompatibility. Biomaterials. 2020;249:120011.
29. Pickard JM, Maurice CF, Kinnebrew MA, Abt MC, Schenten D, Golovkina TV, Bogatyrev SR, Ismagilov RF, Pamer EG, Turnbaugh PJ, Chervonsky AV. Rapid fucosylation of intestinal epithelium sustains host-commensal symbiosis in sickness. Nature. 2014;514:638–41.
30. Adrover JM, McDowell SAC, He XY, Quail DF, Egeblad M. NETworking with cancer: the bidirectional interplay between cancer and neutrophil extracellular traps. Cancer Cell. 2023;41:505–26.
31. Carminita E, Crescence L, Panicot-Dubois L, Dubois C. Role of neutrophils and NETs in animal models of thrombosis. Int J Mol Sci 2022;23(3):1411.
32. Chen Q, Zhang L, Li X, Zhuo W. Neutrophil extracellular traps in tumor metastasis: pathological functions and clinical applications. Cancers (Basel) 2021;13(11):2832.
33. Yang Y, Hu L, Wang C, Yang X, Song L, Jiang C, Li Y, Li T, Liu WT, Feng J. p38/TF/HIF-alpha Signaling Pathway Participates in the Progression of CIPN in Mice. *Biomed Res Int* 2019, 2019:5347804.
34. Stephens M, von der Weid PY. Lipopolysaccharides modulate intestinal epithelial permeability and inflammation in a species-specific manner. Gut Microbes. 2020;11:421–32.
35. Gauthier AE, Rotjan RD, Kagan JC. Lipopolysaccharide detection by the innate immune system May be an uncommon defence strategy used in nature. Open Biol. 2022;12:220146.
36. Xie K, Cheng X, Zhu T, Zhang D. Single-cell transcriptomic profiling of dorsal root ganglion: an overview. Front Neuroanat. 2023;17:1162049.
37. Haberberger RV, Kuramatilake J, Barry CM, Matusica D. Ultrastructure of dorsal root ganglia. Cell Tissue Res. 2023;393:17–36.
38. Areti A, Yerra VG, Naidu V, Kumar A. Oxidative stress and nerve damage: role in chemotherapy induced peripheral neuropathy. Redox Biol. 2014;2:289–95.
39. Yang Y, He Z, Wu S. Ursolic acid alleviates paclitaxel-induced peripheral neuropathy through PPARgamma activation. Toxicol Appl Pharmacol. 2024;484:116883.
40. Lu Y, Zhang P, Zhang Q, Yang C, Qian Y, Suo J, Tao X, Zhu J. Duloxetine attenuates Paclitaxel-Induced peripheral nerve injury by inhibiting p53-Related pathways. J Pharmacol Exp Ther. 2020;373:453–62.
41. Zhang M, Du W, Acklin S, Jin S, Xia F. SIRT2 protects peripheral neurons from cisplatin-induced injury by enhancing nucleotide excision repair. J Clin Invest. 2020;130:2953–65.
42. Choi I, Zhang Y, Seegobin SP, Pruvost M, Wang Q, Purtell K, Zhang B, Yue Z. Microglia clear neuron-released alpha-synuclein via selective autophagy and prevent neurodegeneration. Nat Commun. 2020;11:1386.
43. He F, Huang Y, Song Z, Zhou HJ, Zhang H, Perry RJ, Shulman GI, Min W. Mitophagy-mediated adipose inflammation contributes to type 2 diabetes with hepatic insulin resistance. J Exp Med. 2021;218(3):e20201416.
44. Bonilla DL, Bhattacharya A, Sha Y, Xu Y, Xiang Q, Kan A, Jagannath C, Komatsu M, Eissa NT. Autophagy regulates phagocytosis by modulating the expression of scavenger receptors. Immunity. 2013;39:537–47.
45. Maldonado RF, Sa-Correia I, Valvano MA. Lipopolysaccharide modification in Gram-negative bacteria during chronic infection. FEMS Microbiol Rev. 2016;40:480–93.
46. McBride MJ. Bacteroidetes gliding motility and the type IX secretion system. Microbiol Spectr 2019, 7.
47. Zhao Z, Ning J, Bao XQ, Shang M, Ma J, Li G, Zhang D. Fecal microbiota transplantation protects rotenone-induced Parkinson's disease mice via suppressing inflammation mediated by the lipopolysaccharide-TLR4 signaling pathway through the microbiota-gut-brain axis. Microbiome. 2021;9(1):226.
48. Li W, Deng M, Loughran PA, Yang M, Lin M, Yang C, Gao W, Jin S, Li S, Cai J, et al. LPS induces active HMGB1 release from hepatocytes into exosomes through the coordinated activities of TLR4 and Caspase-11/GSDMD signaling. Front Immunol. 2020;11:229.
49. Platt N, Gordon S. Is the class A macrophage scavenger receptor (SR-A) multifunctional? - The Mouse's Tale. J Clin Invest. 2001;108:649–54.
50. Zhang Z, Jiang Y, Zhou Z, Huang J, Chen S, Zhou W, Yang Q, Bai H, Zhang H, Ben J, et al. Scavenger receptor A1 attenuates aortic dissection via promoting efferocytosis in macrophages. Biochem Pharmacol. 2019;168:392–403.
51. Todt JC, Hu B, Curtis JL. The scavenger receptor SR-A I/II (CD204) signals via the receptor tyrosine kinase Mertk during apoptotic cell uptake by murine macrophages. J Leukoc Biol. 2008;84:510–8.
52. Denorme F, Portier I, Rustad JL, Cody MJ, de Araujo CV, Hoki C, Alexander MD, Grandhi R, Dyer MR, Neal MD et al. Neutrophil extracellular traps regulate ischemic stroke brain injury. J Clin Invest 2022;132(10):e154225.
53. Gao X, Zhao X, Li J, Liu C, Li W, Zhao J, Li Z, Wang N, Wang F, Dong J, et al. Neutrophil extracellular traps mediated by platelet microvesicles promote thrombosis and brain injury in acute ischemic stroke. Cell Commun Signal. 2024;22:50.
54. Simpson BW, Trent MS. Pushing the envelope: LPS modifications and their consequences. Nat Rev Microbiol. 2019;17:403–16.
55. Lai Y, Chen Y, Zheng J, Liu Z, Nong D, Liang J, Li Y, Huang Z. Gut microbiota of white-headed black langurs (Trachypithecus leucocephalus) in responses to habitat fragmentation. Front Microbiol. 2023;14:1126257.
56. Hennell James R, Deme JC, Hunter A, Berks BC, Lea SM. Structures of the type IX secretion/gliding motility motor from across the phylum bacteroidetes. mBio. 2022;13:e0026722.
57. Leng Y, Yi M, Fan J, Bai Y, Ge Q, Yao G. Effects of acute intra-abdominal hypertension on multiple intestinal barrier functions in rats. Sci Rep. 2016;6:22814.
58. Luthuli S, Wu S, Cheng Y, Zheng X, Wu M, Tong H. Therapeutic effects of fucoidan: A review on recent studies. Mar Drugs 2019;17(9):487.
59. Wei Q, Xing M, Wang K, Yang Q, Zhao J, Wang Y, Li X, Ji K, Song S. Fucoidan is not completely dependent on degradation to fucose to relieve ulcerative colitis. Pharmaceuticals (Basel) 2022, 15.
60. Goto Y, Obata T, Kunisawa J, Sato S, Ivanov II, Lamichhane A, Takeyama N, Kamioka M, Sakamoto M, Matsuki T, et al. Innate lymphoid cells regulate intestinal epithelial cell glycosylation. Science. 2014;345:1254009.
61. Tang X, Wang W, Hong G, Duan C, Zhu S, Tian Y, Han C, Qian W, Lin R, Hou X. Gut microbiota-mediated lysophosphatidylcholine generation promotes colitis in intestinal epithelium-specific Fut2 deficiency. J Biomed Sci. 2021;28:20.
62. Coyne MJ, Reinap B, Lee MM, Comstock LE. Human symbionts use a host-like pathway for surface fucosylation. Science. 2005;307:1778–81.
63. Pacheco AR, Curtis MM, Ritchie JM, Munera D, Waldor MK, Moreira CG, Sperandio V. Fucose sensing regulates bacterial intestinal colonization. Nature. 2012;492:113–7.
64. Li Y, Yan H, Zhang Y, Li Q, Yu L, Li Q, Liu C, Xie Y, Chen K, Ye F, et al. Alterations of the gut Microbiome composition and lipid metabolic profile in radiation enteritis. Front Cell Infect Microbiol. 2020;10:541178.

Publisher's note